A growth-factor-activated lysosomal K^+ channel regulates Parkinson's pathology

https://doi.org/10.1038/s41586-021-03185-z

Received: 20 February 2020

Accepted: 10 December 2020

Published online: 27 January 2021

Check for updates

Jinhong Wie[1], Zhenjiang Liu[1], Haikun Song[2], Thomas F. Tropea[3], Lu Yang[4], Huanhuan Wang[4], Yuling Liang[5], Chunlei Cang[1], Kimberly Aranda[1], Joey Lohmann[1], Jing Yang[4], Boxun Lu[2], Alice S. Chen-Plotkin[3]✉, Kelvin C. Luk[5]✉ & Dejian Ren[1]✉

Lysosomes have fundamental physiological roles and have previously been implicated in Parkinson's disease[1–5]. However, how extracellular growth factors communicate with intracellular organelles to control lysosomal function is not well understood. Here we report a lysosomal K^+ channel complex that is activated by growth factors and gated by protein kinase B (AKT) that we term lysoK$_{GF}$. LysoK$_{GF}$ consists of a pore-forming protein TMEM175 and AKT: TMEM175 is opened by conformational changes in, but not the catalytic activity of, AKT. The minor allele at rs34311866, a common variant in *TMEM175*, is associated with an increased risk of developing Parkinson's disease and reduces channel currents. Reduction in lysoK$_{GF}$ function predisposes neurons to stress-induced damage and accelerates the accumulation of pathological α-synuclein. By contrast, the minor allele at rs3488217—another common variant of *TMEM175*, which is associated with a decreased risk of developing Parkinson's disease—produces a gain-of-function in lysoK$_{GF}$ during cell starvation, and enables neuronal resistance to damage. Deficiency in TMEM175 leads to a loss of dopaminergic neurons and impairment in motor function in mice, and a *TMEM175* loss-of-function variant is nominally associated with accelerated rates of cognitive and motor decline in humans with Parkinson's disease. Together, our studies uncover a pathway by which extracellular growth factors regulate intracellular organelle function, and establish a targetable mechanism by which common variants of *TMEM175* confer risk for Parkinson's disease.

Several hundred plasma-membrane ion channels are gated by cellular factors, such as voltage and lipids[6,7]. Protein kinases regulate channels by phosphorylation. Whether they also gate channels independent of catalysis has not been established. Recent studies have revealed several endolysosomal channels[8,9]. Extracellular amino acids inhibit the Na^+- and Ca^{2+}-permeable channels[10], but whether growth factors also communicate with the intracellular channels remains to be determined.

Growth factors activate a lysosomal K^+ channel

In lysosomes dissected from neurons starved in Dulbecco's modified Eagle's medium (DMEM), there was little K^+ current (I_K). Notably, adding a B27 supplement to the medium activated a large I_K. As a control, removing B27 did not reduce Na^+ current (Fig. 1a, b, Extended Data Fig. 1a, b). A major component in B27 is insulin[11]. The application of insulin, brain-derived neurotrophic factor (BDNF) or nerve growth factor (NGF) to starved neurons reactivated I_K (Fig. 1c); thus, neuronal lysosomes have a growth-factor-activated K^+ channel (that is, lysoK$_{GF}$).

TMEM175 forms the lysoK$_{GF}$ pore

The linear current–voltage relationship of lysoK$_{GF}$ is similar to that of the K^+ channel formed by the pore-forming protein TMEM175 (which is localized to the lysosome)[12,13], but distinct from that of the large-conductance Ca^{2+}-activated BK potassium channels[14]. Nontransfected HEK293T cell lysosomes had little I_K (28.0 ± 4.7 pA, at 100 mV, n = 20). Transfecting human TMEM175 generated large K^+ currents ($I_{TMEM175}$) under serum-replete conditions. $I_{TMEM175}$ was abolished by starvation, and was reactivated by refeeding with insulin or serum containing growth factors but not with amino acids or boiled serum (Fig. 1d).

In homozygous *Tmem175*-knockout mice (Fig. 1e, f), lysosomes in neurons from B27-replete medium and starved neurons refed with growth factors lacked substantial I_K (about 5 pA, which is close to the detection limit); this suggests that TMEM175 is the only major K^+ channel under our conditions. In neurons from heterozygote mice, I_K was reduced by around 50%, which suggests strict gene dosage dependency (Fig. 1g–i, Extended Data Fig. 1d).

AKT is necessary for lysoK$_{GF}$

In HEK293T cells (which, unlike neurons, do not express NGF or BDNF receptors[15–17]), only insulin activated TMEM175 (Fig. 1d, Extended Data Fig. 1c), which suggests that growth factors activate TMEM175 indirectly through receptors. A major target of growth factor receptors is the ubiquitously expressed AKT[18]. Incubating cells transfected with human TMEM175 with nonspecific (wortmannin) or specific allosteric

[1]Department of Biology, University of Pennsylvania, Philadelphia, PA, USA. [2]State Key Laboratory of Medical Neurobiology, MOE Frontiers Center for Brain Science, School of Life Sciences, Fudan University, Shanghai, China. [3]Department of Neurology, Perelman School of Medicine, University of Pennsylvania, Philadelphia, PA, USA. [4]School of Life Sciences, IDG/McGovern Institute for Brain Research, Peking University, Beijing, China. [5]Center for Neurodegenerative Disease Research, Department of Pathology and Laboratory Medicine, University of Pennsylvania Perelman School of Medicine, Philadelphia, PA, USA. ✉e-mail: chenplot@pennmedicine.upenn.edu; kelvincl@pennmedicine.upenn.edu; dren@sas.upenn.edu

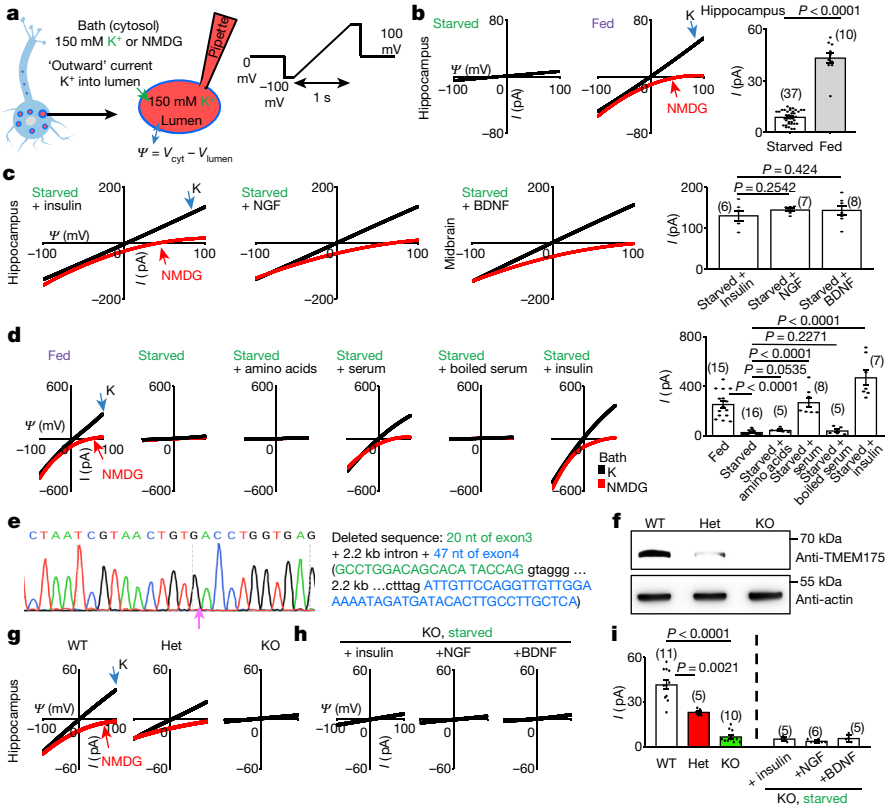

Fig. 1 | A growth-factor-activated lysosomal K^+ channel, lysoK$_{GF}$. **a**, Schematic of the recording of neuronal lysosomes. **b**, Currents (*I*) recorded at varying voltages (*Ψ*) from mouse hippocampal neurons with (starved) or without (fed) overnight starvation in DMEM containing no B27 nutrient. **c**, Currents from neurons with starvation followed by refeeding (in DMEM medium) with insulin (100 nM for 4 h), NGF (100 ng ml^{-1}, 3 h) or BDNF (10 ng ml^{-1}, 3 h). **d**, Reconstituting lysoK$_{GF}$ by TMEM175 transfection in HEK293T cells. Currents were recorded before, 2 h after starvation or after a 2-h starvation followed by refeeding with amino acids (10× for 10 min), with serum (10%, 4 h), with serum inactivated by boiling for 10 min or with insulin (100 nM, 4 h). **e**–**i**, Comparison between lysoK$_{GF}$ from wild-type and TMEM175-knockout neurons. **e**, Sequencing of the knock out, showing deletion of parts of exons 3 and 4. **f**, Total brain proteins (100 µg) from wild type (WT), heterozygous (het) and homozygous TMEM175-knockout (KO) mice were immunoblotted with anti-TMEM175 and—as a loading control—reblotted with anti-actin. For gel source data, see Supplementary Fig. 1. **g**, Currents from B27-replete hippocampal neurons. **h**, Currents from B27-starved (overnight in DMEM) knockout neurons refed with insulin (hippocampal neurons), NGF (hippocampal) or BDNF (midbrain). Black (K) and red (*N*-methyl-D-glucamine (NMDG)) traces are currents recorded with bath solutions containing K^+ or NMDG, respectively. Averaged I_K sizes (at 100 mV, with K^+-containing bath) are in bar graphs (**b**–**d**, **i**). Data are mean ± s.e.m. Numbers of recordings are in parentheses. *P* values shown are from unpaired two-tailed *t*-tests.

AKT inhibitors, cotransfecting a dominant-negative AKT or knocking down AKT all markedly reduced $I_{TMEM175}$ (Fig. 2a, b, f, g), which suggests that AKT is necessary to activate TMEM175.

To test whether AKT is also sufficient for TMEM175 activation, we applied the AKT activator SC79 to patch-clamped lysosomes[19]. In both HEK293T cells transfected with TMEM175 (Fig. 2c–f) and mouse neurons (Fig. 2h, i, Extended Data Fig. 1e), SC79 fully restored $I_{TMEM175}$ from starved cells and activated additional current in nutrient-replete cells. In mouse neurons, MK-2206 inhibited native I_K. SC79 activated no I_K in TMEM175-knockout cells, which suggests that TMEM175 is the only direct lysosomal K^+ channel that is targeted by AKT.

In *Drosophila* S2 cells (which do not have endogenous TMEM175), coexpression of Akt or the application of recombinant AKT protein was required for human TMEM175 to generate robust currents (Extended Data Fig. 2). Together, our data suggest that AKT is obligatory for a functional mammalian TMEM175 channel.

AKT forms a complex with TMEM175

The channel-activating AKT must be bound to a lysosome. Lysosomal AKT interacts with the mTOR–TSC pathway[20,21]. However, SC79 activated TMEM175 even when mTOR was knocked down or inhibited (Extended Data Fig. 3). In mouse brains, human SH-SY5Y cells and transfected HEK293T cells, TMEM175 immunoprecipitated with AKT: this suggests that TMEM175 and AKT form a complex (Fig. 3a, b, Extended Data Fig. 4a).

AKT binds close to the channel pore

TMEM175 has one (in mouse) or two (in human) cytosol-facing relaxed AKT-substrate consensus sites around S241 and T338. The conserved T338 is located in the TM2–TM3 linker of repeat II, in close proximity to the cytosolic end of the pore-forming TM1 helix[22]. Mutating both T338 and S241 or T338 alone—but not the nonconserved S241 alone—to alanine led to markedly reduced I_K, with the channel no longer being potentiated by SC79 (Fig. 3b, c, e, l, Extended Data Fig. 4b–d).

Neutralizing the three charged residues around T338 at the same time, or neutralizing K336 alone, disrupted the AKT–TMEM175 association and eliminated $I_{TMEM175}$ (Fig. 3b, h–j, l). Supporting the idea that AKT binds to the TM2–TM3 linker, the second repeat of TMEM175 associated with AKT (Extended Data Fig. 4e), and a fusion protein containing the 19 amino acids in the linker region—but not the TMEM175(K336A) mutant—pulled down AKT (Fig. 3d).

AKT gates TMEM175 without kinase activity

One way that SC79 might activate TMEM175 is by phosphorylating T338. A T338D substitution had no effect on $I_{TMEM175}$ (Fig. 3b, f, g, l).

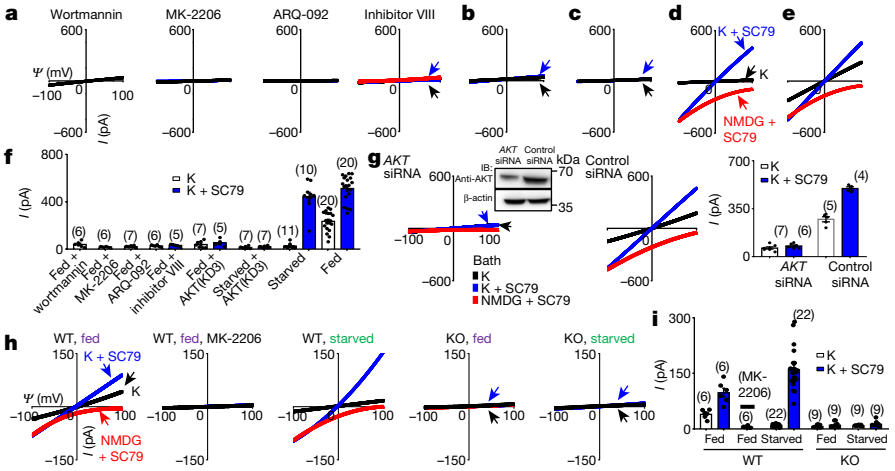

Fig. 2 | AKT is necessary and sufficient to activate TMEM175. a–**f**, Currents from TMEM175-transfected HEK293T cells. In **b**, **c**, a dominant-negative AKT (triple-mutant AKT(K179M/T308A/S473A); AKT(KD3)) was cotransfected. In **a**, cells were pretreated with wortmannin (20 μM, 2 h), an allosteric AKT inhibitor (MK-2206 (20 μM, 3 h) or ARQ-092 (20 μM, 3 h)) or AKT inhibitor VIII (10 μM, 3 h) before lysosomal dissection for recording. In **a**, **b**, **e**, cells were not starved; in **c**, **d**, cells were starved in Hank's balanced salt solution (HBSS) medium for 2 h. **g**, Currents from TMEM175-transfected cells without starvation pretreated with small interfering (si)RNAs against *AKT1*, *AKT2* and *AKT3* or with a control siRNA. Inset, western blot showing the efficient knockdown of AKT. For gel source data, see Supplementary Fig. 1. IB, immunoblot. **h**, **i**, Currents from wild-type and TMEM175-knockout mouse hippocampal neurons before or after starvation (overnight in DMEM). The AKT activator SC79 (10 μM) was applied to the bath during some of the recordings (blue and red traces). Bar graphs in **f**, **g**, **i** show averaged current sizes (at 100 mV). Data are mean ± s.e.m. Numbers of recordings are in parentheses. Arrows are used to indicate curves that overlap and are not easily distinguished. Colours denote conditions for recording: from a bath containing K^+ (black), K^+ and SC79 (blue) or NMDG and SC79 (red).

In addition, our recording bath contained no ATP or Mg^{2+} (which are components that are essential for kinase catalysis) but SC79 activated TMEM175 (Fig. 2d–i). Furthermore, adding Mg-ATP to the bath did not increase $I_{TMEM175}$ (Fig. 3k, l), which suggests that the kinase activity of AKT is unnecessary for activating TMEM175.

In its canonical activation, AKT changes from closed to an open state (in which the pleckstrin homology (PH) domain is released from the catalytic domain) to subsequently phosphorylate its targets[18,23]. Allosteric inhibitors that inhibit this conformational change also blocked $I_{TMEM175}$. By contrast, ATP-competitive kinase inhibitors—which inhibit AKT kinase activity but not the conformational change—had little effect (Fig. 2f, Extended Data Fig. 5). Furthermore, AKT with K179M or T308A/S473A substitutions in the kinase domain that eliminate the kinase activity was as functional as wild-type AKT in supporting $I_{TMEM175}$ (Extended Data Fig. 6a, b).

A bath application of phosphatidylinositol(3,4,5)-trisphosphate (PIP_3), which leads AKT to an open state, was sufficient to activate $I_{TMEM175}$ even in starved lysosomes. Similarly, several mutations in the PH domain that alter the lipid specificity of AKT and/or keep AKT in a constitutively open state also change the lipid sensitivity of $I_{TMEM175}$ and/or lead to a constitutively activated $I_{TMEM175}$ that is resistant to starvation. These findings suggest that conformational changes in AKT alone are sufficient to activate TMEM175 (Extended Data Fig. 6c–e).

TMEM175 requires AKT to stay open

To test whether the association of TMEM175 with AKT is required for the channel to stay open after activation, we developed inhibitors that dissociate AKT from preassembled TMEM175–AKT complex. After the channel was maximally activated by SC79, a bath application of the inhibitors diminished both heterologously expressed and native $I_{TMEM175}$ (Extended Data Fig. 7).

p.M393T causes lysoK$_{GF}$ loss-of-function

Two missense variants in human *TMEM175* have minor allele frequencies of over 5% in the general population: rs34311866 (a 17.5% minor allele frequency) (hereafter referred to as p.M393T) and rs34884217 (7% minor allele frequency). Both of these variants have also previously been associated with the risk, onset and/or progression of Parkinson's disease[24–29], with the minor alleles at rs34311866 and rs34884217 conferring an odd ratio of 1.25 and 0.74, respectively, for developing Parkinson's disease (Fig. 4a).

Compared to the most common form of TMEM175 (with methionine at amino acid position 373; hereater referred to simply as TMEM175), TMEM175(M393T) expressed at a similar level in HEK293T cells (Fig. 4b, c) and also associated with AKT (Extended Data Fig. 4g), but generated smaller (about 40%, $P < 0.0001$) $I_{TMEM175}$ with or without SC79 (Fig. 4d). As with TMEM175, starvation for 1 h eliminated these currents (Fig. 4d). Previous studies have also shown that TMEM175(M393T) is not as efficient as TMEM175 when it is used to restore cellular function in cells in which TMEM175 is knocked down[30].

Most carriers of p.M393T are heterozygous. We recorded lysosomes cotransfected with TMEM175 and TMEM175(M393T) at 1:1 ratio to model the heterozygous state. Compared to that of TMEM175 alone, the $I_{TMEM175}$ generated by the mixture was reduced (by 43% for basal and by 54% for SC79-activated) (Fig. 4d). The simplest explanation is that the mutant has a dominant-negative effect and heterodimeric channels[22,31,32] that contain a wild type and a mutant copy of TMEM175 behave similarly to a homodimeric mutant. Therefore, $I_{TMEM175}$ in heterozygous individuals and in individuals who are homozygous for p.M393T are close to each other, and are similar to a situation in which there is only one copy of functional TMEM175 (heterozygous knockout).

Substituting the M393 of TMEM175 with a bulky residue (M393W) markedly reduced $I_{TMEM175}$. By contrast, replacing M393 with a more-conserved residue (isoleucine)—as found in mouse TMEM175 (I390)—had little effect (Fig. 4b–d).

We also tested the variation in TMEM175(I390T) knock-in mice. I_K values in heterozygous and homozygous neurons were reduced to a similar extent as compared to those in wild-type mice, which again suggests a dominant-negative effect (Extended Data Fig. 8a, b).

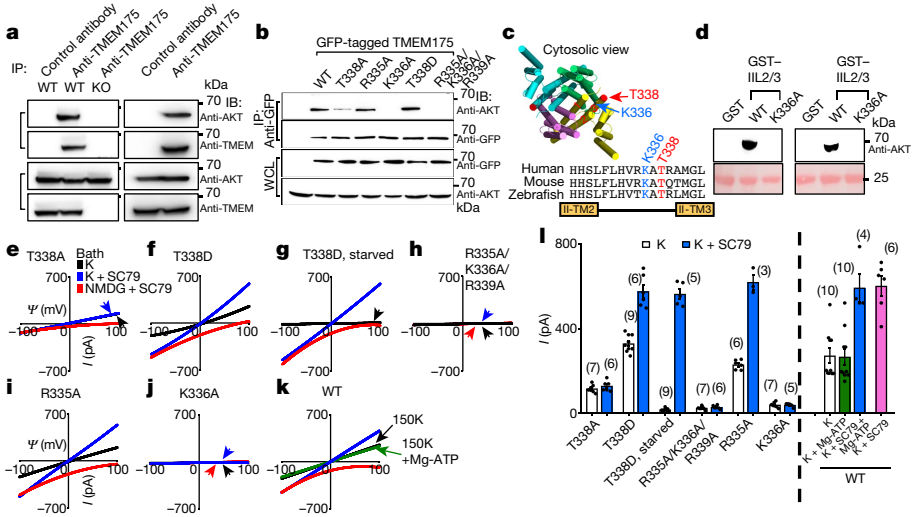

Fig. 3 | AKT activates TMEM175 via catalysis-independent and interaction-dependent mechanisms. a, Association between native TMEM175 and AKT. Top two panels, total proteins prepared from wild-type and TMEM175-knockout mouse brains (lanes 1–3) or SH-SY5Y human neuroblastoma cells (lanes 4 and 5) were immunoprecipitated (IP) with anti-TMEM175 or with a control antibody (anti-UNC79) and blotted with anti-AKT and anti-TMEM175. Bottom two panels, total protein blotted for input control. **b**, Lysates from HEK293T cells transfected with GFP-tagged wild-type or mutant TMEM175 were immunoprecipitated with anti-GFP and blotted with anti-GFP or with anti-AKT. Whole-cell lysates (WCL) were also blotted for input control. **c**, Sequence alignment of the T338 region. The locations of T338 and K336 are indicated on the human TMEM175 structure (Protein Data Bank code (PDB) 6WCA). **d**, Pull down of AKT with human TMEM175–glutathione-*S*-transferase (GST) fusion protein. Cell lysates from human AKT1-transfected HEK293T (lanes 1–3) or S2 (lanes 4–6) cells were incubated with glutathione-agarose-bound GST (as a negative control), GST fusion protein of the 19 amino acids of human TMEM175 containing the wild-type TM2–TM3 linker of domain II (GST–IIL2/3; sequence: HHSLFLHVRKATRAMGLLN) or that with the K336A substitution. Top, bound proteins were probed with anti-AKT (top). Bottom, GST fusion proteins were visualized with Ponceau-S staining of the membrane after immunoblotting. **e**–**j**, Currents recorded from HEK293T cells transfected with TMEM175 mutants as indicated with (**g**) or without starvation (wild type shown in Fig. 2d–f). **k**, Currents recorded with or without Mg-ATP (2 mM) in the bath. **l**, Averaged I_K sizes (at 100 mV) recorded under conditions as indicated. Data are mean ± s.e.m. Numbers of recordings are in parentheses. In **e**–**k**, arrows are used to indicate curves that overlap and are not easily distinguished. For gel source data, see Supplementary Fig. 1.

rs34884217 is a coding variant

In the gnomAD database, rs34884217 is annotated (with uncertainty) as a loss-of-function variant of *TMEM175* with disruption in a splice acceptor (n.206-2A>C) (Fig. 4a). We introduced an equivalent A-to-C substitution in *Tmem175* in mouse and amplified the whole open-reading-frame cDNAs from the wild-type and knock-in brains. There was a single PCR band and only one transcript species, which suggests no aberrant splicing. Instead, the substitution led to a p.Q65P change in TMEM175 (Extended Data Fig. 8e-g). Thus, rs34884217 (hereafter, p.Q65P) is a coding variant.

p.Q65P causes gain-of-function under stress

The Q65 of TMEM175 is conserved between mice and about 93% of humans, but some mammals (including about 7% of humans) have proline at this position (Extended Data Fig. 8h). As with TMEM175 protein, TMEM175(Q65P) associated with AKT (Extended Data Fig. 4g). In transfected cells, TMEM175(Q65P) led to a reduced $I_{TMEM175}$ compared to TMEM175 under serum-replete conditions. However, TMEM175(Q65P) was more resistant to starvation: starving cells for one hour almost completely eliminated the wild-type currents, but had little effect on TMEM175(Q65P) (Fig. 4e).

In wild-type neurons, I_K was eliminated after a 3-h starvation. However, I_K in neurons from homozygous *Tmem175*$^{Q65P/Q65P}$ knock-in mice was intact even after 6 h, and required 9 h to be eliminated (Fig. 4f). The I_K in neurons from heterozygous mice was about 30% smaller than that of wild type under the B27-replete condition but was larger than that of wild type after a 3-h starvation, and required 6 h to be eliminated (Fig. 4f). Thus, p.Q65P is a gain-of-function variant during stress.

LysoK$_{GF}$ regulates lysosomal function

A potential lysosomal function of TMEM175 is to provide counter ions to achieve acidic pH[33]. In TMEM175-knockout neurons, lysosomal pH was about 0.5 units more alkaline upon starvation—in contrast with that of wild type, which remained stable (Extended Data Fig. 9a).

Many lysosomal enzymes (such as cathepsin D (CatD)) work optimally at acidic pH. The amount of mature CatD cleaved from the precursor was lower in TMEM175-knockout neurons than in wild type (Extended Data Fig. 9b, c).

We also used LC3 (an autophagosome marker) labelled with green fluorescent protein (GFP) and red fluorescent protein (RFP) to assay autophagosome–lysosome fusion. Compared to wild-type neurons, TMEM175-knockout neurons showed accelerated fusion and an accumulation of undigested autophagosomes (Extended Data Fig. 9d). Similar differences in lysosomal function between wild-type and TMEM175-deficient cells have previously been observed using knockout cell lines and knockdown rat neurons[12,34].

LysoK$_{GF}$ protects neurons

As variants of TMEM175 are associated with neurodegenerative diseases and AKT is known to protect neurons against stress-induced damage[25,35,36], we tested whether lysoK$_{GF}$ protects neurons using a culture model in which damage can be quantified well[37–39]. Compared to wild type, both homozygous and heterozygous TMEM175-knockout neurons showed much more damage in response to insults, such as the neurotoxin MPTP, reactive oxygen species (H_2O_2) and/or nutrient removal. However, TMEM175(Q65P) neurons had less damage, which suggests that p.Q65P provides additional protection (Extended Data Fig. 10).

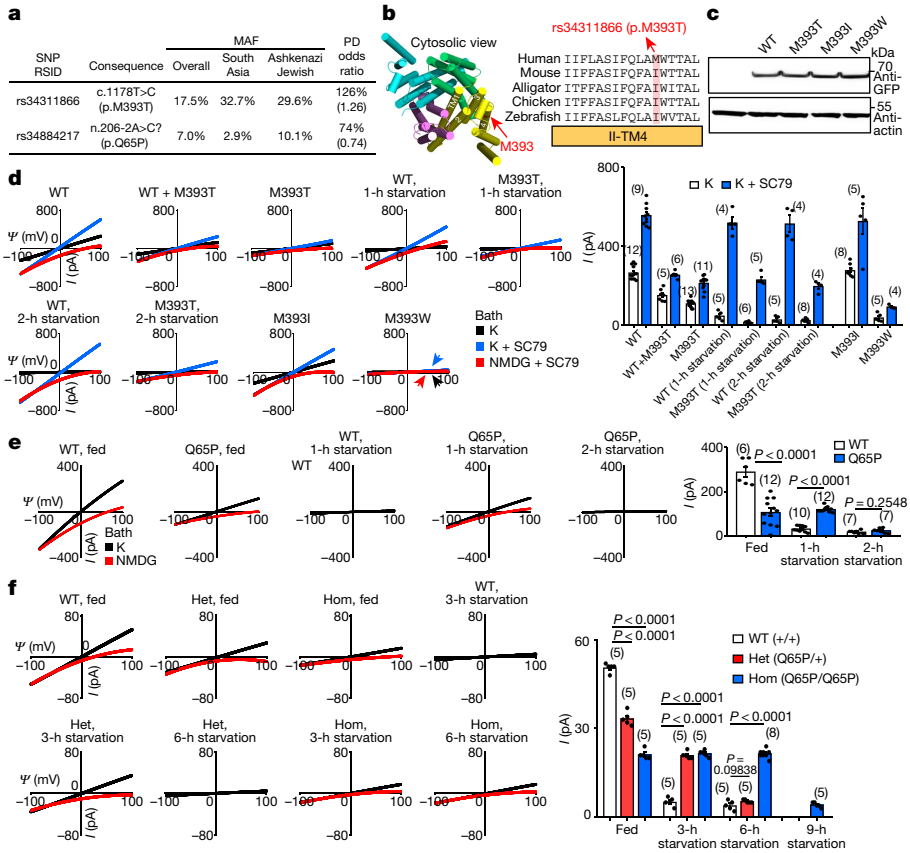

Fig. 4 | Common TMEM175 variants associated with susceptibility to Parkinson's disease bidirectionally regulate function of the lysosomal K_{GF} channel. a, Variants in human *TMEM175* with minor allele frequency (MAF) > 5% (from https://gnomad.broadinstitute.org/). The two single-nucleotide polymorphisms (SNPs) are associated with increased (rs34311866, meta-analysis odds ratio 1.26, 95% confidence interval [1.22, 1.31], $P = 6.00 \times 10^{-41}$) or decreased (rs34884217, odds ratio 0.74, 95% confidence interval [0.69, 0.81], $P = 1.56 \times 10^{-12}$) susceptibility to Parkinson's disease (PD)[25] (data from http://www.pdgene.org/). **b**–**d**, Characterization of p.M393T. **b**, Sequence alignments of M393 region (indicated on structure PDB 6WCA). **c**, Protein expression levels of wild type and human TMEM175 mutants. Total protein from nontransfected HEK293T cells (lane 1) and cells transfected with GFP-tagged wild-type or mutant human TMEM175 (lanes 2–5) was probed with anti-GFP or anti-actin (for input control). For gel source data, see Supplementary Fig. 1. **d**, Currents from HEK293T cells transfected with wild-type and/or mutant TMEM175 with or without starvation in HBSS medium for 1 or 2 h, as indicated. **e**, **f**, Characterization of the TMEM175(Q65P) variant in HEK293T cells (**e**) and knock-in mouse neurons (**f**). **e**, Currents from wild-type and TMEM175(Q65P) cDNA-transfected HEK293T cells before (0 h, fed) or after (1 or 2 h) starvation. **f**, Currents from wild-type (+/+), heterozygous (Q65/+, het) and homozygous (Q65P/Q65P, hom) knock-in mouse midbrain neurons before (0 h, fed) or after (3, 6 or 9 h) starvation in DMEM. In **d**–**f**, averaged I_K sizes (at 100 mV) are shown in the bar graphs. Data are mean ± s.e.m. Numbers of recordings are in parentheses. *P* values shown are for unpaired two-tailed *t*-tests.

α-Synuclein accumulation in mutant neurons

Intraneuronal inclusions (Lewy pathology) comprising misfolded α-synuclein (α-syn) hyperphosphorylated at S129 are a hallmark of Parkinson's disease[40,41]. Upon entering neurons, pathogenic α-syn recruits endogenous α-syn to form Parkinson's-disease-like inclusions[42,43]. The internalization of extracellular α-syn occurs via the endolysosomal pathway, and lysosomal clearance may slow down the prion-like propagation of α-syn[44–46]. In an in vitro transmission model in which α-syn preformed fibrils were used to seed endogenous α-syn into Lewy-like inclusions, neurons from the homozygous and heterozygous TMEM175-knockout and TMEM175(I390T) knock-in mice all accumulated markedly increased α-syn phosphorylated at S129 two weeks after exposure, compared to wild type (Fig. 5a, Extended Data Fig. 8d)—consistent with previous findings in cultured rat neurons upon TMEM175 knockdown[34]. The accumulation of α-syn also led to increased damage to the integrity of lysosomal membranes in the TMEM175-knockout neurons, as assayed using recruitment of galectin 3[47] (Extended Data Fig. 9e). Although mouse and neuronal models do not fully phenocopy the pathologies of Parkinson's disease, the findings do suggest that even a partial reduction in TMEM175 (by about 50%) exacerbates the formation of pathogenic α-syn.

Dopaminergic neuron loss in TMEM175-knockout mice

We examined whether loss of TMEM175 leads to a reduced survival of midbrain dopaminergic neurons, which represent a vulnerable subpopulation in Parkinson's disease. Whereas the numbers of tyrosine-hydroxylase-positive neurons between aged wild-type and TMEM175-knockout mice were comparable in the ventral tegmental area, TMEM175-knockout mice showed a decrease of these neurons in the substantia nigra pars compacta (Fig. 5b).

Using a more sensitive assay with optically cleared tissue and whole-brain image reconstruction, we tested whether a milder reduction (of about 50%) in TMEM175 affects dopaminergic neurons. Compared to wild type, heterozygote mice had a small (about 10%) but significant reduction in the number of dopaminergic neurons and a reduction in the size (around 20%) and the axon density (around 10%) of dopaminergic nerve bundles projecting from the substantia nigra pars compacta to the striatum (Fig. 5c).

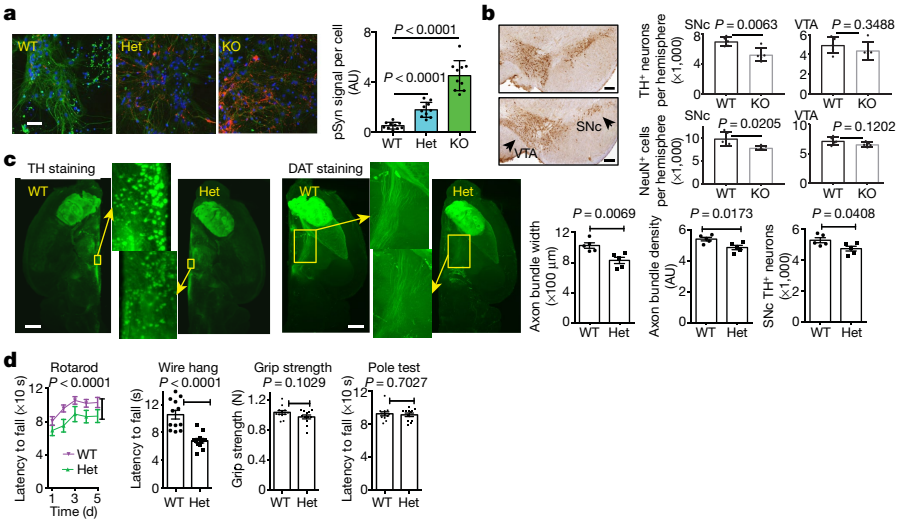

Fig. 5 | LysoK$_{GF}$ deficiency leads to accelerated spreading of pathogenic α-syn, loss of dopaminergic neurons and impaired motor function in mice. **a**, α-Syn spread assay. Cultured mouse hippocampal neurons were seeded with α-syn preformed fibrils and immunostained two weeks later with anti-pSer129 α-syn (pSyn, red), α-tubulin (green) and DAPI (blue). Bar graph shows pSyn signals normalized to the number of cells (n = 10 coverslips). Scale bar, 50 μm. AU, arbitrary units. **b**, Loss of dopaminergic neurons in TMEM175-knockout mice. Left, tyrosine hydroxylase (TH) immunostaining at the level of ventral tegmental area (VTA) and substantia nigra pars compacta (SNc) from wild-type (top) and homozygous TMEM175-knockout (bottom) littermates (18–22 months old). n = 5 mice for each genotype. Right, quantification of TH-positive neurons and total NeuN-positive cells. Scale bars, 200 μm. **c**, Brains from wild-type and heterozygous littermates (about 12 months old; n = 5 mice for each genotype) were whole-tissue immunolabelled with anti-TH or anti-dopamine transporter (DAT) and imaged with light-sheet microscopy. Bar graphs show the numbers of dopaminergic neurons and width of axonal bundles. Scale bars, 1 mm. **d**, Behavioural tests using wild-type and heterozygous littermates (about 12 months old). n = 12 mice for each test. In **a**–**d**, P values given are from two-tailed t-tests, except for rotarod in **d** (two-way analysis of variance).

Impaired motor skills in mutant mice

In behavioural assays, heterozygote TMEM175-knockout mice performed significantly more poorly than their wild-type littermates in rotarod and wire-hang tests, but showed no obvious deficiency in grip strength and pole tests (Fig. 5d). These findings suggest that mice with haploinsufficiency retain basic muscle function, but are impaired in tasks that require more coordination.

Effects of p.M393T in Parkinson's disease

We examined a cohort of 341 longitudinally followed (median of 4.08 years, up to a maximum of 12) patients with Parkinson's disease at the University of Pennsylvania[48] (genotypes in panel 1, Extended Data Fig. 10f). In patients with longitudinal cognitive data who did not have dementia at baseline (n = 313 out of 341), p.M393T was associated with the rate of cognitive decline in an additive genetic model (β = 0.453, two-tailed nominal P = 0.003), with p.M393T carriers declining more rapidly than individuals without this variant (panel 2 in Extended Data Fig. 10f). In minor allele dominant models in which carriers of one or two p.M393T variants are considered to be equivalent, we obtained virtually indistinguishable results (β = 0.527, two-tailed nominal P = 0.005)—echoing our cellular findings that having one copy of this variant may be near equivalent to having two. Controlling for *GBA*-variant carrier status (identified in 14 participants; p.E365K, n = 4; p.N409S, n = 4; p.L483P, n = 4; p.R496H, n = 1; and p.R202*, n = 1) had no effect on these results (β = 0.451, two-tailed nominal P = 0.004).

In patients with longitudinal motor data (n = 336 out of 341), p.M393T was also associated significantly with the rate of motor decline in an additive genetic model (β = −0.345, two-tailed nominal P = 0.032): p.M393T carriers declined more rapidly than those without this variant (panel 3 in Extended Data Fig. 10f). Controlling for *GBA*-variant carrier status had no effect on these results (β = −0.341, two-tailed nominal P = 0.038).

Finally, we assessed the international Parkinson's Progression Marker Initiative (PPMI) cohort, which enrolled 423 participants with newly diagnosed Parkinson's disease from 33 clinical sites in 13 countries, for replication of our results. As the cohort is enrolled at diagnosis, cognitive change (usually a later symptom) is minimal; however, over a median follow-up time of five years, PPMI participants with Parkinson's disease do show worsening motor function. In 373 participants who have available clinical and genetic data, p.M393T genotypes trended towards association with the rate of motor decline in an additive model (β = −0.322, two-tailed P = 0.066), with p.M393T carriers again declining more rapidly than those without the variant (panel 4 in Extended Data Fig. 10f).

Discussion

We have discovered a growth-factor-activated, kinase-gated lysosomal ion channel, identified the subunits of this channel, elucidated a catalysis-independent channel-gating mechanism by a kinase (Extended Data Fig. 7e), revealed a function in neuronal protection in mice and susceptibility to Parkinson's disease pathology in humans, and delineated the molecular consequences of two high-frequency genetic variants that are associated with susceptibility to Parkinson's disease. AKT protects neurons against a wide spectrum of cellular insults[18,49,50]. AKT receives inputs from numerous growth factors and other stimuli, providing a mechanism by which environmental cues are coupled to lysosomal function. As *TMEM175* variants associated with Parkinson's disease risk are commonly present in the general population (with minor allele frequencies of p.M393T as high as 30% in some ethnic groups), our findings shed light on a considerable proportion of Parkinson's disease risk in the human population. In addition, enhanced lysoK$_{GF}$ function—as in p.Q65P-carrying neurons—provides added protection against stress-induced damage and is associated with a decreased risk of developing Parkinson's disease. As such, the channel complex may be an attractive target for the development of drugs to alleviate neurodegenerative diseases.

Online content

Any methods, additional references, Nature Research reporting summaries, source data, extended data, supplementary information, acknowledgements, peer review information; details of author contributions and competing interests; and statements of data and code availability are available at https://doi.org/10.1038/s41586-021-03185-z.

1. Ballabio, A. & Bonifacino, J. S. Lysosomes as dynamic regulators of cell and organismal homeostasis. *Nat. Rev. Mol. Cell Biol.* **21**, 101–118 (2020).
2. Laplante, M. & Sabatini, D. M. mTOR signaling in growth control and disease. *Cell* **149**, 274–293 (2012).
3. Wong, Y. C., Kim, S., Peng, W. & Krainc, D. Regulation and function of mitochondria-lysosome membrane contact sites in cellular homeostasis. *Trends Cell Biol.* **29**, 500–513 (2019).
4. Lie, P. P. Y. & Nixon, R. A. Lysosome trafficking and signaling in health and neurodegenerative diseases. *Neurobiol. Dis.* **122**, 94–105 (2019).
5. Abeliovich, A. & Gitler, A. D. Defects in trafficking bridge Parkinson's disease pathology and genetics. *Nature* **539**, 207–216 (2016).
6. Hille, B. *Ion Channels of Excitable Membranes*, 3rd Edn (Sinauer Associates, 2001).
7. Jan, L. Y. & Jan, Y. N. Voltage-gated potassium channels and the diversity of electrical signalling. *J. Physiol.* **590**, 2591–2599 (2012).
8. Xu, H. & Ren, D. Lysosomal physiology. *Annu. Rev. Physiol.* **77**, 57–80 (2015).
9. Cang, C., Bekele, B. & Ren, D. The voltage-gated sodium channel TPC1 confers endolysosomal excitability. *Nat. Chem. Biol.* **10**, 463–469 (2014).
10. Cang, C. et al. mTOR regulates lysosomal ATP-sensitive two-pore Na^+ channels to adapt to metabolic state. *Cell* **152**, 778–790 (2013).
11. Brewer, G. J., Torricelli, J. R., Evege, E. K. & Price, P. J. Optimized survival of hippocampal neurons in B27-supplemented neurobasal, a new serum-free medium combination. *J. Neurosci. Res.* **35**, 567–576 (1993).
12. Cang, C., Aranda, K., Seo, Y. J., Gasnier, B. & Ren, D. TMEM175 is an organelle K^+ channel regulating lysosomal function. *Cell* **162**, 1101–1112 (2015).
13. Chapel, A. et al. An extended proteome map of the lysosomal membrane reveals novel potential transporters. *Mol. Cell Proteomics* **12**, 1572–1588 (2013).
14. Cao, Q. et al. BK channels alleviate lysosomal storage diseases by providing positive feedback regulation of lysosomal Ca^{2+} release. *Dev. Cell* **33**, 427–441 (2015).
15. El-Shewy, H. M., Lee, M. H., Obeid, L. M., Jaffa, A. A. & Luttrell, L. M. The insulin-like growth factor type 1 and insulin-like growth factor type 2/mannose-6-phosphate receptors independently regulate ERK1/2 activity in HEK293 cells. *J. Biol. Chem.* **282**, 26150–26157 (2007).
16. Anderson, E. M. et al. BDNF–TrkB controls cocaine-induced dendritic spines in rodent nucleus accumbens dissociated from increases in addictive behaviors. *Proc. Natl Acad. Sci. USA* **114**, 9469–9474 (2017).
17. Perreault, M. et al. Activation of TrkB with TAM-163 results in opposite effects on body weight in rodents and non-human primates. *PLoS ONE* **8**, e62616 (2013).
18. Manning, B. D. & Toker, A. AKT/PKB signaling: navigating the network. *Cell* **169**, 381–405 (2017).
19. Jo, H. et al. Small molecule-induced cytosolic activation of protein kinase Akt rescues ischemia-elicited neuronal death. *Proc. Natl Acad. Sci. USA* **109**, 10581–10586 (2012).
20. Arias, E. et al. Lysosomal mTORC2/PHLPP1/Akt regulate chaperone-mediated autophagy. *Mol. Cell* **59**, 270–284 (2015).
21. Menon, S. et al. Spatial control of the TSC complex integrates insulin and nutrient regulation of mTORC1 at the lysosome. *Cell* **156**, 771–785 (2014).
22. Oh, S., Paknejad, N. & Hite, R. K. Gating and selectivity mechanisms for the lysosomal K^+ channel TMEM175. *eLife* **9**, e53430 (2020).
23. Ebner, M., Lucic, I., Leonard, T. A. & Yudushkin, I. PI(3,4,5)P3 engagement restricts Akt activity to cellular membranes. *Mol. Cell* **65**, 416–431 (2017).
24. Blauwendraat, C. et al. Parkinson's disease age at onset genome-wide association study: defining heritability, genetic loci, and α-synuclein mechanisms. *Mov. Disord.* **34**, 866–875 (2019).
25. Nalls, M. A. et al. Large-scale meta-analysis of genome-wide association data identifies six new risk loci for Parkinson's disease. *Nat. Genet.* **46**, 989–993 (2014).
26. Krohn, L. et al. Genetic, structural and functional evidence link *TMEM175* to synucleinopathies. *Ann. Neurol.* **87**, 139–153 (2020).
27. Iwaki, H. et al. Genetic risk of Parkinson disease and progression: an analysis of 13 longitudinal cohorts. *Neurol. Genet.* **5**, e348 (2019).
28. Lill, C. M. et al. Impact of Parkinson's disease risk loci on age at onset. *Mov. Disord.* **30**, 847–850 (2015).
29. Davis, A. A. et al. Variants in *GBA*, *SNCA*, and *MAPT* influence Parkinson disease risk, age at onset, and progression. *Neurobiol Aging* **37**, 209.e1–209.e7 (2016).
30. Jinn, S. et al. Functionalization of the TMEM175 p.M393T variant as a risk factor for Parkinson disease. *Hum. Mol. Genet.* **28**, 3244–3254 (2019).
31. Lee, C. et al. The lysosomal potassium channel TMEM175 adopts a novel tetrameric architecture. *Nature* **547**, 472–475 (2017).
32. Brunner, J. D. et al. Structural basis for ion selectivity in TMEM175 K^+ channels. *eLife* **9**, e53683 (2020).
33. Steinberg, B. E. et al. A cation counterflux supports lysosomal acidification. *J. Cell Biol.* **189**, 1171–1186 (2010).
34. Jinn, S. et al. TMEM175 deficiency impairs lysosomal and mitochondrial function and increases α-synuclein aggregation. *Proc. Natl Acad. Sci. USA* **114**, 2389–2394 (2017).
35. Aleyasin, H. et al. DJ-1 protects the nigrostriatal axis from the neurotoxin MPTP by modulation of the AKT pathway. *Proc. Natl Acad. Sci. USA* **107**, 3186–3191 (2010).
36. Humbert, S. et al. The IGF-1/Akt pathway is neuroprotective in Huntington's disease and involves Huntingtin phosphorylation by Akt. *Dev. Cell* **2**, 831–837 (2002).
37. Niu, J. et al. 2′,3′-Dideoxycytidine protects dopaminergic neurons in a mouse model of Parkinson's disease. *Neurochem. Res.* **42**, 2996–3004 (2017).
38. Sakamoto, S., Miyara, M., Sanoh, S., Ohta, S. & Kotake, Y. Mild MPP^+ exposure-induced glucose starvation enhances autophagosome synthesis and impairs its degradation. *Sci. Rep.* **7**, 46668 (2017).
39. Whittemore, E. R., Loo, D. T., Watt, J. A. & Cotman, C. W. A detailed analysis of hydrogen peroxide-induced cell death in primary neuronal culture. *Neuroscience* **67**, 921–932 (1995).
40. Goedert, M., Spillantini, M. G., Del Tredici, K. & Braak, H. 100 years of Lewy pathology. *Nat. Rev. Neurol.* **9**, 13–24 (2013).
41. Fujiwara, H. et al. α-Synuclein is phosphorylated in synucleinopathy lesions. *Nat. Cell Biol.* **4**, 160–164 (2002).
42. Luk, K. C. et al. Pathological α-synuclein transmission initiates Parkinson-like neurodegeneration in nontransgenic mice. *Science* **338**, 949–953 (2012).
43. Volpicelli-Daley, L. A. et al. Exogenous α-synuclein fibrils induce Lewy body pathology leading to synaptic dysfunction and neuron death. *Neuron* **72**, 57–71 (2011).
44. Gao, J., Perera, G., Bhadbhade, M., Halliday, G. M. & Dzamko, N. Autophagy activation promotes clearance of α-synuclein inclusions in fibril-seeded human neural cells. *J. Biol. Chem.* **294**, 14241–14256 (2019).
45. Karpowicz, R. J. Jr et al. Selective imaging of internalized proteopathic α-synuclein seeds in primary neurons reveals mechanistic insight into transmission of synucleinopathies. *J. Biol. Chem.* **292**, 13482–13497 (2017).
46. Davis, A. A., Leyns, C. E. G. & Holtzman, D. M. Intercellular spread of protein aggregates in neurodegenerative disease. *Annu. Rev. Cell Dev. Biol.* **34**, 545–568 (2018).
47. Aits, S. et al. Sensitive detection of lysosomal membrane permeabilization by lysosomal galectin puncta assay. *Autophagy* **11**, 1408–1424 (2015).
48. Tropea, T. F. et al. *TMEM106B* effect on cognition in Parkinson disease and frontotemporal dementia. *Ann. Neurol.* **85**, 801–811 (2019).
49. Thomas, B. et al. Resistance to MPTP-neurotoxicity in α-synuclein knockout mice is complemented by human α-synuclein and associated with increased β-synuclein and Akt activation. *PLoS ONE* **6**, e16706 (2011).
50. Datta, S. R., Brunet, A. & Greenberg, M. E. Cellular survival: a play in three Akts. *Genes Dev.* **13**, 2905–2927 (1999).

Methods

No statistical methods were used to predetermine sample size. The experiments were not randomized, and—in some experiments (see Reporting Summary)—investigators were not blinded to allocation during experiments and outcome assessment.

Mice

Mouse use was approved by the University of Pennsylvania Institutional Animal Care and Use Committee. TMEM175-knockout, TMEM175(Q65P) knock-in and TMEM175(I390T) knock-in mouse lines were generated using CRISPR–Cas9 methods, as previously described[51]. The knockout line was generated with two single-guide RNAs (sgRNAs) with target sequences of ttctaatcgtaactgtggcc **tgg** (exon 3) and tacacttgccttgct caacc **tgg** (exon 4) (protospacer adjacent motif sequences in bold). The mutation deletes part of exons 3 and 4 (starting at the codon that encodes A88 in the second transmembrane domain), resulting in an out-of-frame truncation (Fig. 1e). For the generation of TMEM175(Q65P) knock-in line, the sgRNA target was complementary of (**cct** agcaactag gatcgctgtct) and the single-strand (ss)DNA donor had the sequence of complementary of (gtgctatagggtgagtcttgccattgaaatgaccactgttgg atcgtgtgttactttgttctaatagcagtgttcttttcatacagccgtttgacaaaagtatacaga aactgctagcaactaggatcgctgtctacctcatgacatttctaatcgtaactgtggcctggaca gcacataccaggtagggaattagacct). For the generation of the TMEM175(I390T) knock-in line, the sgRNA was gcatcttcca gtttgccatc **tgg** and the ssDNA donor had the sequence of cttgagcgtgtgcgtgtcagctgt gccatcatcttctttgccagcatcttccagtttgccacgtggactacagccctgctgcatcagac agaaacactgcagccagctgtgcaatttggtggg. *Cas9* RNA and sgRNAs were synthesized using in vitro transcription with MEGAshortscript T7 kit (Thermo Fisher Scientific, no. AM1354, for sgRNAs) or mMESSAGE mMACHINE T7 ULTRA kit (Thermo Fisher Scientific, no. AM1345, for *Cas9* RNA) and purified using the MEGAclear kit (Thermo Fisher Scientific, no. AM1908). *Cas9* RNA, sgRNA and, for knock-in, donor DNA were co-injected into embryos (done by the Transgenic and Chimeric Mouse Core of the University of Pennsylvania). Embryos used for injection were collected from B6SJLF1/J mice for the TMEM175-knockout and C57BL6/J (JAX) mice for the TMEM175(Q65P) and TMEM175(I390T) knock-in lines. F_0 founders were crossed to C57BL6/J (JAX) mice to obtain germline transmission. Three independent sublines were used for each line. The TMEM175-knockout and knock-in mice are viable, fertile and do not have obvious gross abnormalities. Mice used for neuronal culture studies had been backcrossed to C57BL6/J mice for more than 5 generations for TMEM175(Q65P) and the TMEM175-knockout, and 1–2 generations for TMEM175(I390T). Knockout mice used for behavioural studies were made from mice backcrossed to C57BL6/J mice for more 10 generations. Littermates were used as controls. The sample sizes were not predetermined. All the mouse uses in Fig. 5 were blinded. The mouse numbers in the behavioural studies in Fig. 5c were randomized before studies.

Cell culture

Mammalian cells were maintained at 37 °C and 5% CO_2. *Drosophila* S2 cells were maintained at room temperature. HEK293T (from ATCC), SH-SY5Y (from ATCC) and S2 (from Gibco) cells were authenticated by the providers and were not further authenticated. Cells were cultured in DMEM (Thermo Fisher Scientific, no. 11965084, for HEK293T), DMEM and F12 (1:1 for SH-SY5Y cells (DMEM from Thermo Fisher Scientific, no. 11965084; F12 from Lonza, no. 12-615F), or Schneider's *Drosophila* medium (Thermo Fisher Scientific, no. 21720024 for S2 cells), supplemented with 10% fetal bovine serum (R&D Systems, no. S11150) and 1× penicillin–streptomycin (Thermo Fisher Scientific, no. 15140122). For neuronal culture, hippocampal, midbrain and cortical neurons were dissociated from mouse brains at postnatal day 0 and digested with filtered papain (Worthington, no. LS003119) as previously described[52,53]. Neurons were plated on poly-L-lysine-coated 12-mm coverslips in 80% DMEM (Lonza, no. 12-709F), 10% Ham's F12 (Lonza, no. 12-615F), 10% bovine calf serum (Thermo Fisher Scientific, no. SH30073.03) and 0.5× penicillin–streptomycin. Medium was changed the next day (day in vitro 1) to neurobasal-A medium (Thermo Fisher Scientific, no. 10888022) supplemented with 1× B27 supplement (Thermo Fisher Scientific, no. 17504044), L-glutamate (25 μM), 0.5 mM GlutaMAX Supplement (Thermo Fisher Scientific, no. 35050061) and 1× penicillin–streptomycin, and—on day in vitro 2—to neurobasal A medium supplemented with 1× B27 supplement, 0.5 mM GlutaMAX supplement and 1× penicillin–streptomycin. The HBSS medium used for HEK293T cell starvation contained (in mM) 110 NaCl, 45 $NaHCO_3$, 5 KCl, 2 $CaCl_2$ and 1 $MgCl_2$ (pH 7.4). Starvation for patch-clamp recording was about 2 h unless otherwise stated. Longer starvation times (4 h or overnight) tested also eliminated $I_{TMEM175}$.

Plasmid DNA constructs

For HEK293T cell expression, the human TMEM175 used for transfection has previously been described[12]. Yellow fluorescent protein (YFP) or GFP was attached at the N-terminal of human TMEM175 for the identification of transfected lysosomes for patch-clamp recording. The anti-GFP antibody used in the studies also recognizes YFP. Human AKT1 (Flag and haemagglutinin (HA)-tagged, Addgene no. 9021) and the dominant-negative form of AKT (triple mutant K179M/T308A/S473A, Addgene no. 9031) were from Addgene and were cloned in pcDNA3-based vector. Point mutations were introduced using the Gibson Assembly Cloning Kit (New England Biolabs, no. E5510S) and were confirmed with Sanger sequencing.

For expression in *Drosophila* S2 cells, human AKT1 was cloned into the BamHI (blunted with Klenow polymerase-mediated filling) and EcoRI sites of the pIZT/V5-based vector. The GFP-fused human TMEM175 was cloned into the KpnI (blunted with Klenow) and EcoRI sites of the pIZT/V5-based vector.

For the production of GST fusion proteins used in the GST pull-down assays in Fig. 3d, cDNA encoding wild-type human TMEM175 peptide (amino acids 327–345) (HHSLFLHVRKATRAMGLLN, DNA insert sequenceGGATCCCACCACTCACTCTTCCTGCATGTGCGCAAGGCCACG CGGGCCATGGGGCTGCTGAACTAGGAATTC) or the corresponding K336A mutant (HHSLFLHVRAATRAMGLLN, DNA insert sequence GGATCCCACCACTCACTCTTCCTGCATGTGCGCGCGGCCACGCGGGC CATGGGGCTGCTGAACTAGGAATTC) was cloned into the BamHI and EcoRI sites of the pGEX-6P-2 vector.

Transfection

HEK293T cells were transfected using PolyJet (Signa Gen, no. SL100688) transfection reagent. *Drosophila* S2 cells were transfected using X-tremeGENE HP DNA transfection reagent (Roche, no. 6366244001). Transfected cells were replated on 12-mm poly-L-lysine-coated coverslips about 48 h after transfection. Neurons were transfected between day in vitro 5 and 7 using Lipofectamine LTX reagent with PLUS reagent (Thermo Fisher Scientific, no. 15338100).

Electrophysiology

Whole-organelle patch-clamp recordings from lysosomes enlarged to about 3 μm with vacuolin 1 treatment were performed at room temperature, as previously described[10,12]. Each lysosome selected for recording was dissected out using a sharp glass pipette (illustrated in Fig. 1a). For neurons, lysosomes in soma were selected. All recordings were carried out using a ramp protocol (−100 mV to 100 mV in 1 s, Ψ_{hold} = 0 mV, as illustrated in the right subpanel of Fig. 1a). Ψ is the voltage across lysosomal membrane, with lumen as the reference[54]. Outward K^+ current (positive) denotes the movement of K^+ out of the cytosol (bath) into the lumen. For transfected cells, recordings were done 48–60 h after transfection. To record I_K, pipette solution contained (in mM) 145 K-methanesulfonate, 5 KCl and 10 MES (pH 5.5). Unless otherwise stated, bath solutions contained (in mM) 145

K-methanesulfonate, 5 KCl and 10 HEPES (pH 7.2). In the $NMDG^+$ bath, K^+ was replaced with $NMDG^+$ (a large ion that is impermeable to the channel). For TPC Na^+ current recordings in Extended Data Fig. 3e–h, bath solutions contained (in mM) 140 K-gluconate, 4 NaCl, 2 $MgCl_2$, 0.39 $CaCl_2$, 1 EGTA, 10 HEPES (pH adjusted to 7.2 with KOH) and 0.001 $PI_{(3,5)}P_{(2)}$ (water soluble diC8 form, from Echelon Biosciences, no. P-3508). The pipette solution contained (in mM) 145 NaCl, 5 KCl, 1 $MgCl_2$, 2 $CaCl_2$, 10 HEPES, 10 MES and 10 glucose (pH adjusted to 4.6 with NaOH). Some of the currents recorded, especially small ones around the reversal potential, may have partial contribution from endogenous lysosomal H^+ and Cl^- currents.

For whole-cell recording from S2 cells, the pipette solution contained (in mM) 150 KOH, 2.5 $MgCl_2$ and 10 HEPES (pH 7.2). Pipette solution in some recordings in Extended Data Fig. 2h, as indicated, also contained recombinant human AKT1 protein (from Sino Biological, no. 10763-H08B). The bath solution contained (mM) 150 KOH, 10 TEA, 3 HCl, 1 $MgCl_2$ and 10 HEPES (pH 7.2). In the NMDG-containing bath, K^+ was substituted with NMDG-methanesulfonate. Recordings were carried out using a ramp protocol (−100 mV to 100 mV in 1 s, V_{hold} = 0 mV).

Recordings were performed with a MultiClamp 700B Microelectrode Amplifier controlled with pClamp and Clampfit (version 10.4, Molecular Devices), used for data collection and processing. All electrophysiological recordings were repeated in at least two preparations.

Immunoprecipitation, GST pull down and western blotting

Primary antibodies used were anti-β-actin (rabbit monoclonal, Cell Signaling Technology, no. 4970, for Figs. 1f, 2g, 4c, Extended Data Figs. 5b, 6a, 9b, used at 1:3,000 dilution for western blot), anti-GFP (mouse monoclonal, Thermo Fisher Scientific, no. A11120, for Figs. 3b, 4c, Extended Data Figs. 4a, d, f, g, 7b, used at 1:1,000 dilution for western blot; mouse monoclonal, Santa Cruz Biotechnology, no. sc-9996, for Extended Data Fig. 4e, used at 1:2,000 dilution for western blot), anti-TMEM175 (rabbit polyclonal, Proteintech, no. 19925-1-AP, for Figs. 1f, 3a, used at 1:1,000 for western blot), anti-TMEM175 (rabbit polyclonal, Origene, no. TA335429, for Fig. 3a, used at 2 μg ml^{-1} for immunoprecipitation), anti-Akt (rabbit polyclonal, Cell Signaling Technology, no. 9272, for Fig. 3d, Extended Data Fig. 2d, used at 1:1,000 dilution for western blot), anti-Pan AKT (mouse monoclonal, R&D Systems, no. MAB2055, for Figs. 2g, 3a, b, Extended Data Figs. 4f, g, 5b, 6a, used at 0.2 μg ml^{-1} for western blot), anti-HA (mouse monoclonal, Santa Cruz Biotechnology, no. sc-7392, for Extended Data Figs. 4a, d, e, 7b, used at 1:1,000 dilution for western blot), anti-phospho-AKT (Ser473) (rabbit polyclonal, Cell Signaling Technology, no. 9271, for Extended Data Figs. 4f, 5b, a, used at 1:2,000 dilution for western blot), anti-phospho-AKT (Thr308) (rabbit monoclonal, Cell Signaling Technology, no. 4056, for Extended Data Figs. 4f, 5b, 6a, used at 1:1,000 dilution for western blot), anti-phospho-GSK3β (Ser9) (rabbit monoclonal, Cell Signaling Technology, no. 9323, for Extended Data Figs. 5b, 6a, used at 1:1,000 dilution for western blot), anti-GSK3β (rabbit monoclonal, Cell Signaling Technology, no. 9315, for Extended Data Figs. 5b, 6a, used at 1:1,000 dilution for western blot), anti-phospho-PRAS40(T246) (rabbit monoclonal, Cell Signaling Technology, no. 2691, for Extended Data Figs. 5b, 6a used at 1:1,000 dilution for western blot), anti-PRAS40 (rabbit monoclonal, Cell Signaling Technology, no. 2997, for Extended Data Figs. 5b, 6a used at 1:1,000 dilution for western blot), anti-CatD (rabbit polyclonal, Cell Signaling Technology, no. 2284, for Extended Data Fig. 9b, used at 1:200 dilution for western blot). HRP-conjugated secondary antibodies used for western blot were anti-rabbit IgG (Cell Signaling Technology, no. 7074, for Figs. 1f, 3d, 4c, Extended Data Figs. 2d, 5b, 6a, 9b, used at 1:4,000 dilution), and anti-mouse IgG for immunoprecipitation (Abcam, no. ab131368, used at 1:1,000 dilution for Fig. 3a, b, Extended Data Figs. 4a, d–g, 7b; Cell Signaling Technology, no. 7076, used at 1:4,000 dilution for Figs. 3b, 4c, Extended Data Figs. 4d, e, 7b), VeritBlot for immunoprecipitation detection reagent (HRP) (Abcam, no. ab131366, used at 1:4,000 dilution for Fig. 3a, Extended Data Fig. 4f). Protein A agarose used for immunoprecipitation was from Thermo Fisher Scientific (no. 15918).

For HEK293T, SH-SY5Y and *Drosophila* S2 cells used in Figs. 2g, 3a, b, d, 4c, Extended Data Figs. 2d, 4a, d–g, 5b, 6a, 7b, cells from a 35-mm dish were lysed for 30 min with 400 μl immunoprecipitation buffer containing (in mM) 50 Tris-HCl (pH 7.4), 150 NaCl, 0.1% NP-40 and 1 EDTA, supplemented with EDTA-free protease inhibitor cocktail (PIC, Roche, no. 11873580001). In Extended Data Figs. 4f, 5b, 6a, lysis buffer was also supplemented with phosphatase inhibitor (PhosStop, Roche, no. 4906837001). Lysate was centrifuged at 20,000*g* for 30 min at 4 °C. Sixty μl of the supernatant was taken out as input. The rest was mixed with 1 μg antibody and incubated at 4 °C for 2 h. Samples were mixed with buffer-equilibrated protein A–agarose at 4 °C for 2 h, spun down (2,000*g*, 3 min), and washed with immunoprecipitation buffer (3 times, 5 min each). Proteins were eluted for 15 min at 70 °C with 30 μl 1× lithium dodecyl sulfate (LDS) sample buffer (diluted from 4× with immunoprecipitation buffer) supplemented with 100 mM DTT.

For mouse brain protein used in Figs. 1f, 3a, each brain was homogenized in 1 ml homogenization buffer (5 mM Tris pH7.4 and 250 mM sucrose) with PIC, mixed for 1 h and spun at 1,000*g* for 10 min at 4 °C. Protein concentration was measured using the BCA protein assay kit (Thermo Fisher Scientific, no. 23227). For the immunoprecipitation experiment in Fig. 3a, 1 mg total protein was solubilized in a final volume of 500 μl immunoprecipitation buffer (diluted from 2× immunoprecipitation buffer) at 4 °C for 1 h, followed by spinning at 20,000*g* for 30 min at 4 °C. The supernatant was transferred to a new tube and incubated with 1 μg antibody at 4 °C for 2 h, followed by mixing with buffer-equilibrated protein A–agarose overnight at 4 °C. Proteins were spun down (2,000*g*, 3 min), washed with immunoprecipitation buffer (3× 5 min), and were eluted for 15 min at 70 °C with 30 μl 1× LDS sample buffer supplemented with 100 mM DTT. Thirty μg of each total protein was loaded as input.

For western blotting in Fig. 1f, an equal amount (50 μg) of protein from each brain was loaded. For immunoprecipitation in Extended Data Fig. 7b, aliquots of total lysate from HEK293T cells was mixed with 10 μM peptide for 2 h at 4 °C before immunoprecipitation.

For the development of peptide inhibitors, the peptides were synthesized at 4-mg scale with >90% purity (Genscript). They were dissolved at 10 mM in ddH_2O (for peptides 4 and 5) or DMSO (for peptides 1, 2 and 3).

For the production of GST fusion proteins used for the GST pull-down assay (Fig. 3d), protein expression in 50 ml of BL21(DE3) bacteria transformed with the corresponding DNA was induced with 0.1 mM IPTG for about 3 h at 30 °C. Cells were lysed with B-Per buffer (Thermo Fisher Scientific, no. 78248), and the protein was purified using glutathione-conjugated sepharose (GE Healthcare, no. 17-0756-01). An aliquot of the glutathione-sepharose-bound GST fusion protein was eluted with glutathione and used to estimate the protein concentration. The remaining sepharose-bound protein was used for the pull-down assays.

Cell lysates containing AKT proteins used in the pull-down assays were prepared from transfected HEK293T and S2 cells. HEK293T cells were transformed with HA-tagged human AKT1 (Addgene plasmid no. 9021). For expression in *Drosophila* S2 cells, cells were transfected with the HA-tagged human AKT1 subcloned into the pIZT-based vector. Transfected cells were spun down at 1,000*g* for 5 min. HEK293T cells were washed once with cold PBS. Cells from each 35-mm dish were lysed with 400 μl immunoprecipitation buffer for 30 min. Lysate was centrifuged at 20,000*g* for 30 min at 4 °C. Sixty μl supernatant was saved as input and 340 μl was transferred to a new tube. Ten μg of agarose-conjugated GST fusion protein was mixed with the 340 μl cell lysate for 2 h at 4 °C and washed with immunoprecipitation buffer 3 times (5 min each). Proteins were eluted with 30 μl 1× LDS sample buffer with 100 mM DTT and used for western blot analysis.

For western blot, proteins were separated using NuPage 4–12% Bis-Tris gels (Thermo Fisher Scientific, no. NP0335) with MOPS SDS

running buffer (Novex, no. NP0001), and transferred onto polyvinylidene difluoride (PVDF) membranes for 1.5 h at 100 V using the Bio-Rad Mini Trans-Blot system. Membranes were preblocked with 5% nonfat dry milk in PBS with 0.1% Tween-20 (PBST) and incubated with primary antibodies at 4 °C overnight. Following 2× washes (5 min each) with PBST, membranes were incubated with HRP-conjugated secondary antibody for 1 h at room temperature, followed by 5× washes (5 min each) and additional incubation with detection reagents (Hi/Lo Digital-ECL western blot detection kit from Kindle Biosciences, no. R1004). Signals were detected with a camera (Fujifilm corporation digital camera (X-A2)). At least three independent repeats were performed for all biochemical experiments.

RNA isolation and reverse-transcription PCR

Total RNA from mouse brains and S2 cells were isolated using RNeasy Mini Kit (Qiagen, no. 74104). First strand cDNA synthesis was performed with 500 ng of total RNA using the SuperScript III Reverse Transcriptase (Thermo Fisher Scientific, no. 18080093) with poly-T primers following the manufacturer's instruction.

For reverse-transcription PCR (RT–PCR) of mouse TMEM175 used in Extended Data Fig. 8f, nested PCR was performed using two pairs of specific primers. The primer pair used for the first PCR had sequences of 5′ATGTCCAGGCTCCAGACTGAGGA3′ (forward primer) and TTAGCAGGGGTCAGGCAAGAGC (reverse). The sequences for the primer pair used in the nested PCR were GCAGGCAGTGGATTCC GAG (forward) and CACTGAAATCTGCATGAGGTGG (reverse). For the first round of PCR, 25-µl reactions were carried out using Phusion high-fidelity DNA polymerase (New England Biolabs, no. M0530), dNTP mix (Thermo Fisher Scientific, no. N8080260, 2.5 mM each) and Phusion HF buffer (New England Biolabs, no. B0518) for 20 cycles (30 s at 94 °C, 30 s at 60 °C, and 1 min 40 s at 72 °C). One µl of the first PCR product was used as input for the second round of PCR (50 µl, 30 cycles, performed under the same cycling condition as in the first PCR). The PCR products of about 1.3 kb were gel-purified using SpinSmart columns (Denville Scientific, no. CM-500-50) and used for Sanger sequencing.

S2 cell *Akt* knockdown with double-strand RNA

Double-strand (ds)RNA against *Drosophila Akt* (also known as *Akt1*) was produced using in vitro RNA synthesis. To generated the DNA template for RNA synthesis, *Drosophila Akt* DNA was amplified using nested PCR with S2 cell first-strand cDNA as template. The primers used for the first PCR had sequences of TCAATAAACACAACTTTCGACCTCA (forward) and CGATGCGAGACTTGTGGAA (reverse). The primers used for the nested PCR had T7 sequence attached at the 5′ end and had sequences of TAATACGACTCACTATAGGGAGCGTTACATCGGGTCATGC (forward, T7 sequence underlined) and TAATACGACTCACTATAGG GATACTAATGTGCGACGAGGTG (reverse). For the first round of nested PCR, a 25-µl reaction was carried out using Phusion high-fidelity DNA polymerase (New England Biolabs, no. M0530), dNTP mix (Thermo Fisher Scientific, no. N8080260, 2.5 mM each) and Phusion HF buffer (New England Biolabs, no. B0518) for 20 cycles (30 s at 94 °C, 30 s at 55 °C, and 1 min 50 s at 72 °C). One µl of the first PCR product was used as template for second PCR (50 µl, 35 cycles of (30 s at 94 °C, 30 s at 64 °C and 1 min 50 s at 72 °C)). The nested PCR product of about 1.6 kb was gel-purified using the QIAquick Gel Extraction Kit (Qiagen, no. 28704). Sanger sequencing and restriction digestion (with BspEI) were performed to ensure the specificity of the DNA.

The *Drosophila Akt* dsRNA was synthesized using the MEGAscript T7 Kit (Thermo Fisher Scientific, no. AM1334) with the purified PCR product as template as previously described[55,56]. The dsRNA product was ethanol-precipitated and resuspended in nuclease-free water. For *Drosophila Akt* knockdown, 15 µg of dsRNA was added to each 35-mm dish on day 1. For cDNA (human TMEM175 and AKT1) transfection with *Drosophila Akt* knockdown, cells were transfected using X-tremeGENE HP DNA transfection reagent 24 h after the addition of dsRNA (on day 2). Cells were collected after 72 h (on day 4) of dsRNA treatment for biochemistry experiments and patch clamping.

AKT knockdown in HEK293T cells with siRNAs

AKT siRNAs and control RNA were from Dharmacon (*AKT1*: L-003000-00-0005, *AKT2*: L-003001-00-0005, *AKT3*: L-003003-00-0005, control: D-001810-10-05). Cells were transfected using Lipofectamine 3000 transfection reagent (Thermo Fisher). *AKT1*, *AKT2* and *AKT3* siRNA or control siRNA (25 nM each, final concentration) was added to each well of a 24-well plate or a 35-mm dish for 24 h.

Neuronal damage, α-syn pathology seeding and galectin 3 assays

For the neuronal damage assay used in Extended Data Fig. 8c, Extended Data Fig. 10, hippocampal and midbrain neurons cultured on 12-mm poly-lysine coated coverslips were transfected with GFP for 48 h for the visualization of neuronal processes. Transfected neurons were treated with stimuli for the duration as indicated. Treated cells were washed 3 times with PBS and fixed with 4% paraformaldehyde (in PBS) for 20 min at room temperature, followed by 5× washes with PBS. Samples were mounted with ProLong Diamond Antifade Mountant (Thermo Fisher Scientific, no. P36965). Images were taken using a Nikon Eclipse Ti inverted microscope-based spinning disc confocal microscope with a 20× lens and a 488-nm laser with an emission filter of 525-nm/50-nm bandwidth (for GFP). Damaged neuronal areas were calculated using ImageJ. Blebs and fragmentation were counted as neuronal damage. The damage index was calculated as the ratio of damaged area to the total neuronal area[57–59].

For α-syn seeding assay and galectin 3 assay (Fig. 5a, Extended Data Fig. 8d), mouse α-syn preformed fibrils (PFFs) were prepared as previously described[60,61], and stored at −80 °C. Before use, PFFs were diluted in PBS (33 ng ml^{-1}) and sonicated for 10 cycles (30-s on and 30-s off) at high power using a Bioruptor Plus (Diagenode). Fifteen µl of PFF solution was added per well in cultures maintained in 24-well plates. After 14 days of treatment, medium was removed and coverslips were washed with PBS. Cells were fixed and permeabilized for 15 min with a mixture of 1% Triton X-100, 4% paraformaldehyde and 4% sucrose at room temperature, followed by 5× washes with PBS. Permeabilized cells were blocked with 3% BSA in 0.1% Triton X-100 for 15 min and incubated with antibody against pSer129 α-syn (mouse monoclonal antibody clone 81A[62]; 1:8,000 in 3% BSA) and, in the galectin assay, with anti-galectin 3 (rat monoclonal, 1:100 diluted, Santa Cruz Biotechnology, no. sc-81728[63,64]) in blocking buffer (3% BSA in PBS) for 2 h at room temperature, followed by 5× washes with PBS. Cells were then incubated with Alexa-Fluor-594-conjugated goat anti-mouse secondary antibody (Thermo Fisher Scientific, no. A-11032, diluted to 2 µg ml^{-1} final in blocking buffer) and Alexa-Fluor-488-conjugated rabbit anti-α-tubulin antibody (Cell Signaling Technology, no. 5063S, 1:200 diluted), or, for the galectin 3 assay, Alexa-Fluor-488-conjugated rabbit anti-rat secondary antibody (Thermo Fisher Scientific, no. A-21210, diluted to 2 µg ml^{-1} final in blocking buffer) for 2 h, and washed with PBS (5 times). Coverslips were mounted onto glass slides with ProLong Gold antifade mounting reagent with DAPI (Thermo Fisher Scientific, no. P36935). Images were taken using a Nikon Eclipse Ti inverted microscope-based spinning disc confocal microscope with a 20× lens using a 543-nm laser (emission 645/75, for RFP), a 488-nm laser (emission 525/50, for GFP) and a 405-nm laser (emission 460/50, for DAPI).

Autophagosome–lysosome fusion assay

Autophagosome–lysosome fusion assay was carried out in cultured hippocampal cells transfected with the mCherry- and GFP-tagged LC3[12]. Cells were in DMEM, with or without starvation (B-27 removal overnight). Images were taken using a Nikon Eclipse Ti inverted microscope-based spinning disc confocal microscope using a 543-nm

laser (for RFP) and a 488-nm laser (for GFP). The numbers of mCherry- and/or GFP-positive punta in each cell were counted using ImageJ.

Lysosome pH imaging

Cells plated on glass cover slips, with or without starvation (in DMEM overnight), were loaded with LysoSensor Yellow/Blue DND-160 (Thermo Fisher, no. L7545) for 5 min (1 μM). Cells were washed with imaging buffer containing (in mM) 140 NaCl, 3 KCl, 2 K_2HPO_4, 1 $CaCl_2$, 1 $MgSO_4$ and 5 HEPES (pH 7.4). For the nonstarved group, washing buffer was supplemented with 1× amino acid (Thermo Fisher no. 11130051). Images were taken using a Nikon Eclipse Ti inverted microscope-based spinning disc confocal microscope with a 60× objective, with excitation 405 nm and emission at 460 nm (50-nm bandwidth) and 525 nm (50-nm bandwidth). Calibrations were performed for each cover slip at the end of imaging. Isotonic K^+ solutions containing (in mM) 5 NaCl, 155 KCl, 1.2 MgSO4, 10 glucose, and 25 HEPES supplemented with 10 μM of nigericin and monensin with pH ranging from 4.0 to 7.0 were used as pH-standard solutions. The fluorescence intensity ratios (460 nm/525 nm) obtained with pH-standard solutions were fitted to a Boltzmann sigmoid curve to obtain the pH-standard curve. The pH of each lysosome was calculated by fitting to the standard curve.

Pepstatin A assay

Cells plated on glass cover slips were loaded 1 μM BODIPY FL pepstatin A (Thermo Fisher Scientific, no. P12271) for 1 h at 37 °C and DAPI (Millipore Sigma, no. D9542) for 5 min, followed by washes with PBS (5 times). Cover slips were mounted onto glass slides with ProLong Gold antifade mounting reagent (Thermo Fisher Scientific, no. P36961). Images were taken using a Nikon Eclipse Ti inverted microscope-based spinning disc confocal microscope with a 488-nm laser (emission 525/50 for pepstatin) and a 405-nm laser (emission 460/50 for DAPI). Neuronal areas were calculated using ImageJ (as in the α-syn seeding assays).

Whole-tissue immunolabelling, optical clearing and light-sheet 3D imaging

Mouse brains were fixed with trans-cardiac perfusion. In brief, each mouse was deeply anaesthetized with pentobarbital sodium (70 mg per kg body weight via intraperitoneal injection) was perfused with 25 ml PBS containing 50 μg ml^{-1} heparin, followed by another 25 ml PBS containing 50 μg ml^{-1} heparin, 1% PFA and 10% sucrose. The brain was dissected out, post-fixed in PBS containing 1% PFA at 4 °C for 24 h with gentle shaking, followed by 3× washes (30 min each) with PBS with gentle shaking. Fixed brains were stored in PBS containing 0.02% NaN_3 at 4 °C before immunolabelling and optical clearing.

Whole-tissue immunolabelling and optical clearing was performed following the iDISCO method[65]. All the incubation steps were performed with gentle rotating. Unsectioned fixed brain hemispheres were incubated at room temperature with 20% methanol (diluted in ddH_2O) for 2 h, 40% methanol for 2 h, 60% methanol for 2 h, 80% methanol for 2 h and 100% methanol for 2 h. The tissues were decolorized at 4 °C with a mixture of 30% H_2O_2 and 100% methanol (1:10, v-v) for 48 h, followed by incubation at room temperature with 80% methanol for 2 h, 60% methanol for 2 h, 40% methanol for 2 h, 20% methanol for 2 h and PBS for 2 h.

The tissues were permeabilized at 37 °C with PBS, 0.2% TritonX-100, 0.1% deoxycholate, 10% DMSO and 10 mM EDTA (pH 8.0) overnight, followed by blocking overnight at 37 °C with PBSTE (PBS, 0.2% Triton X-100 and 10 mM EDTA-Na (pH 8.0)] supplemented with 5% normal donkey serum and 10% DMSO. Blocked tissues were immunolabelled at 37 °C for 72 h with the intended primary antibody (1:500 diluted, rat anti-DAT, Santa Cruz Biotechnology, no. sc-32258; rabbit anti-TH, Millipore Sigma, no. AB-152) in PBSTE supplemented with 10 μg ml^{-1} heparin and 5% normal donkey serum, washed at 37 °C with PBSTE supplemented with 10 μg ml^{-1} heparin for 12 h, with buffer changed every 2 h, followed by immunolabelling at 37 °C for 72 h with corresponding Alexa-Fluor-conjugated secondary antibodies (1:500 diluted, goat anti-rat IgG, Alexa 647, Thermo Fisher Scientific, no. A21247; goat anti-rabbit IgG Alexa 647, Thermo Fisher Scientific, no. A21245) in PBSTE supplemented with 10 μg ml^{-1} heparin and 5% normal donkey serum. The tissues were further washed at 37 °C for 48 h with PBSTE supplemented with 10 μg ml^{-1} heparin, with buffer changed every 8 h.

The immunolabelled tissues were incubated at room temperature with 20% methanol (diluted in ddH_2O) for 1 h twice, 40% methanol for 2 h, 60% methanol for 2 h, 80% methanol for 2 h, and 100% methanol for 2 h twice. The tissues were then incubated at room temperature with a mixture of dichloromethane and methanol (2:1, v:v) for 2 h twice and 100% dichloromethane for 1 h three times. The tissues were finally incubated at room temperature with 100% dibenzyl-ether for 12 h three times to become optically cleared.

The optically cleared tissues were imaged on a LaVision Biotec Ultramicroscope II equipped with an sCMOS camera (Andor Neo) and a 2×/NA0.5 objective (MVPLAPO) covered with a 10-mm working-distance dipping-cap. The ImSpector Microscope Controller (Version 144) software was supported by LaVision Biotec. The tissues were immersed in the imaging chamber filled with 100% dibenzyl-ether. For imaging at 1.26× (0.63× zoom) magnification, each tissue was scanned by three combined light sheets from the right side with a step size of 4 μm. The image stacks were acquired using the continuous light sheet scanning method without the contrast-blending algorithm.

Imaris (https://imaris.oxinst.com/packages) was used to reconstruct the image stacks obtained from the light-sheet imaging. For the display purpose, a gamma correction of 1.5 was applied to the raw data. Orthogonal projections of the image stacks were generated for the representative 3D images in the figures. Because single DAT-positive axons within the medial forebrain bundle could not be accurately counted at the resolution of light-sheet imaging, we used the width and fluorescence density of axonal bundles to estimate the loss of dopaminergic projections. The width of the axonal bundle at 1 mm anterior to the substantia nigra was manually measured in the reconstructed 3D image of each brain in Imaris. The fluorescence of the axonal bundle at 1 mm anterior to the substantia nigra was quantified in the orthogonal 3D projection image of each brain, with the background signal taken from the area immediately outside the bundle and subtracted by ImageJ. For the quantification of dopaminergic neurons, the TH-positive neurons located in the substantia nigra were manually counted in the reconstructed 3D image of each brain in Imaris.

Immunohistochemistry for midbrain dopamine neurons

For immunohistochemistry used in Fig. 5b, mouse brains were fixed in 4% PFA overnight following trans-cardiac perfusion and then transferred to PBS for sectioning. Forty-μm-thick floating sections in the coronal plane were prepared using a Compresstome (VF-310; Precisionary Instruments). A series containing every fifth section through the rostrocaudal extent of the substantia nigra and VTA were incubated in PBS containing 0.3% H_2O_2 and 50% methanol for 30 min, and then washed 3× in PBS (with 0.1% Tween 20). Blocking was achieved by a 1.5-h incubation in PBS containing 30% fetal bovine serum and 0.3% Triton-X100. After overnight incubation with primary antibody against either TH (Millipore Sigma, no. TH-16; 1:5,000 in blocking buffer) or NeuN (Millipore Sigma, no. A60; 1:1,000 in blocking buffer), sections were washed 3× in PBS/Tween 20 and transferred to biotinylated anti-mouse IgG (1:1,000; Vector Laboratories, no. BA2000), sections were washed 3× in PBS/Tween 20 and transferred to biotinylated anti-mouse IgG (1:1,000; Vector Laboratories, no. BA2000). Signal was developed using the Vectastain Elite ABC HRP kit (Vector Laboratories, no. PK-6100) as per manufacturer's instructions. Sections were counterstained with haematoxylin and mounted onto Superfrost Plus slides and coverslipped in Cytoseal (Thermo Fisher Scientific). Mounted sections were digitized at 20× (Lamina scanner, PerkinElmer) and the number of TH-positive neurons or NeuN-positive nuclei within the substantia nigra and VTA quantified from each section.

Mouse behavioural tests

Mice were group-housed (up to 5 adult mice per cage) in individually vented cages with a 12-h light/dark cycle. Littermates were used as controls. Experiments were carried out following the guidelines published by the Association for Assessment and Accreditation of Laboratory Animal Care. The Animal Care and Use Committee of the School of Medicine at Fudan University approved the protocols used in mouse experiments. All the behavioural experiments were performed during the light phase. A test sequence was established for mice using a computer-generated pseudo-random number. The experimentalists were blinded to the mouse genotype and original label until after the measurements. Both males and female mice were used. All the mice were kept in the behavioural test room, which was under dim red light, for one hour before the start of the experiments. The test protocols were modified based on previously described methods: open field, rotarod and novel object recognition tests[66,67], grip strength test[67–69], wire hang test[70], tail suspension test[71] and pole test[72]. All the tests were performed under red light, except that for open field instrument, which its own white light.

Rotarod test. Mice were pretrained for 3 consecutive days before the test on a rotarod rotating at 4 rpm for 2 min. They were then tested for 5 days at an accelerating speed (4 to 40 rpm in 2 min), followed by a constant speed of 40 rpm, with a maximum test time of 5 min. Each performance was recorded as the time (in seconds) spent on the rotating rod until the mouse fell off or until the end of the test task. Each test included three repetitions, with an intertrial interval of 60 min to reduce stress and fatigue. The means from the three runs were analysed for each mouse.

Wire hang test. The wire hang test was designed to assess motor function. Each mouse was placed on the metal wire cage top. The cage top was then inverted and placed about 50 cm above the surface of the soft bedding in the home cage, and was manually shaken at a constant speed (4 times per second) in the air. The latency to when the mouse fell from the cage top to which it hung was recorded. Each test was performed with three trials with 3-h intertrial intervals. The performance is presented as the average of the three trials.

Pole test. A climbing frame was placed in a basin filled with about 20-cm depth of water (15 °C). Each mouse was placed about 30 cm above the water on a plexiglass rod (0.8-cm diameter, 80-cm long with 20 cm submerged in H_2O and 60 cm above the water surface). The time when the mouse fell from the plexiglass rod was recorded. Each test included three repetitions, with an intertrial interval of 60 min to reduce stress and fatigue. The means from the three trials were analysed for each mouse.

Grip strength test. Before testing, grip training was performed for each mouse to stimulate the grip reflection and to train it to grasp the force measurement crossbar of the instrument to ensure that it could achieve a stable grip for the measurement of forearm grip strength. The mouse was lifted by the tail and, when the two forelimbs were close to the crossbar, it was induced to actively grasp the crossbar with the claws. The acceptable grip standard was that the mouse could actively stretch the claws, hold the rod smoothly, and did not have dodge, limb distortion or resistance. Grip training was run daily for approximately 5–10 min for 3–5 days until it was able to readily perform a double forelimb grip. After the mouse was able to perform a satisfactory grip, the baseline grip strength when the mouse was at a horizontal position with claws grasping the cross bar was measured by gently lifting the mouse by tail close to the crossbar to induce it to actively grasp the claws to the crossbar. The mouse was then pulled back in the horizontal direction until it was pulled off the crossbar, at which the grip force at the crossbar was measured to reflect the largest double forelimb grip strength of the mouse in resisting pulling. The measurement was recorded three times, with one hour between each measurement to avoid mouse fatigue. The mean values were used for each test.

Human clinical studies

The clinical studies were approved by the University of Pennsylvania (UPenn) Institutional Review Board. Informed consent was obtained at study enrolment. Subjects were enrolled at the UPenn Parkinson's Disease and Movement Disorders Clinic with a clinical diagnosis of Parkinson's disease as previously reported[73]. At enrolment and at each subsequent visit, clinical information was obtained and Mattis Dementia Rating Scale-2 (DRS, $n = 313$)[74] to assess cognition and the Unified Parkinson's Disease Rating Scale Part III (UPDRS-3, $n = 336$) to assess motor function were administered at least at yearly intervals. Subjects with a diagnosis of dementia at enrolment, based on a consensus cognitive diagnosis assigned by pairs of experienced physician raters as previously described[75], were excluded from DRS analysis, as their advanced cognitive impairment at enrolment makes further cognitive testing unreliable. Clinical assessments and neuropsychiatric testing were performed by trained research staff. At enrolment, blood was obtained from all participants, genomic DNA was extracted and genotype at the *TMEM175* index SNP rs34311866 was determined using real-time allelic discrimination with applied Biosystems TaqMan probes, as previously described[76]. Variants in *GBA* were identified by a number of methods, depending on time period, all previously described. These included sequencing the entire coding region ($n = 213$)[77], using a custom targeted next-generation sequencing panel for neurodegenerative diseases (MIND-seq, $n = 19$)[73], or genotyping the SNPs rs76763715 (p.N409S), rs2230288 (p.E365K), rs421016 (p.L483P) or rs80356771 (p.R520C). Four participants only had genotyping data available for rs76763715, and genetic data were missing for two participants.

Statistical analysis of clinical data. Descriptive statistics were calculated for baseline demographics and cognitive testing using available data. Linear mixed-effects[78] were used to test for associations between *TMEM175* genotype and DRS or UPDRS-3 over time (in years), with covariates of age, sex, and disease duration in various genetic models. The mixed effects model controls for variable follow-up time and variable intervals between follow-up visits. A random intercept was included in each mixed-effects model to account for correlations among repeated measures. Statistical tests were two-sided, and alpha was set at 0.05. All statistical analysis was performed in R (http://www.r-project.org). Data and R-scripts are available from the corresponding authors [upon request.

Other statistical information and reproducibility

Origin 8.0 software was used for all electrophysiology data analyses. Data were compared using unpaired two-tailed *t*-test, or one-way analysis of variance test between two or more groups, unless otherwise stated. *P* values with various tests are also given in the Source Data associated with each figure. Numeric data were represented as mean ± s.e.m. Electrophysiological recordings were repeated in at least two independent preparations. Protein chemistry was repeated at least three times.

Reporting summary

Further information on research design is available in the Nature Research Reporting Summary linked to this paper.

Data availability

Gel pictures used to generate the immunoblot data and PCR results are available in Supplementary Fig. 1. Raw electrophysiological recording data used to generate the current-voltage relationship curves

and all other data are available from the corresponding authors upon request. Websites with related data are as follows: PPMI database, www.ppmi-info.org/data; Genome Aggregation Database (gnomAD), https://gnomad.broadinstitute.org/; PD Gene database, http://www.pdgene.org/; and PDB 6WCA, https://www.rcsb.org/structure/6WCA. Source data are provided with this paper.

51. Yang, H., Wang, H. & Jaenisch, R. Generating genetically modified mice using CRISPR/Cas-mediated genome engineering. *Nat. Protoc.* **9**, 1956–1968 (2014).
52. Lu, B. et al. The neuronal channel NALCN contributes resting sodium permeability and is required for normal respiratory rhythm. *Cell* **129**, 371–383 (2007).
53. Lu, B. et al. Extracellular calcium controls background current and neuronal excitability via an UNC79–UNC80–NALCN cation channel complex. *Neuron* **68**, 488–499 (2010).
54. Bertl, A. et al. Electrical measurements on endomembranes. *Science* **258**, 873–874 (1992).
55. Kao, L. R. & Megraw, T. L. RNAi in cultured *Drosophila* cells. *Methods Mol. Biol.* **247**, 443–457 (2004).
56. Clemens, J. C. et al. Use of double-stranded RNA interference in *Drosophila* cell lines to dissect signal transduction pathways. *Proc. Natl Acad. Sci. USA* **97**, 6499–6503 (2000).
57. Gerdts, J., Sasaki, Y., Vohra, B., Marasa, J. & Milbrandt, J. Image-based screening identifies novel roles for IκB kinase and glycogen synthase kinase 3 in axonal degeneration. *J. Biol. Chem.* **286**, 28011–28018 (2011).
58. Sasaki, Y., Vohra, B. P., Lund, F. E. & Milbrandt, J. Nicotinamide mononucleotide adenylyl transferase-mediated axonal protection requires enzymatic activity but not increased levels of neuronal nicotinamide adenine dinucleotide. *J. Neurosci.* **29**, 5525–5535 (2009).
59. Wiemerslage, L. & Lee, D. Quantification of mitochondrial morphology in neurites of dopaminergic neurons using multiple parameters. *J. Neurosci. Methods* **262**, 56–65 (2016).
60. Luk, K. C. et al. Molecular and biological compatibility with host alpha-synuclein influences fibril pathogenicity. *Cell Rep.* **16**, 3373–3387 (2016).
61. Volpicelli-Daley, L. A., Luk, K. C. & Lee, V. M. Addition of exogenous α-synuclein preformed fibrils to primary neuronal cultures to seed recruitment of endogenous α-synuclein to Lewy body and Lewy neurite-like aggregates. *Nat. Protoc.* **9**, 2135–2146 (2014).
62. Waxman, E. A. & Giasson, B. I. Specificity and regulation of casein kinase-mediated phosphorylation of α-synuclein. *J. Neuropathol. Exp. Neurol.* **67**, 402–416 (2008).
63. Angelim, M. K. S. C. et al. Embryonic macrophages and microglia ablation alter the development of dorsal root ganglion sensory neurons in mouse embryos. *Glia* **66**, 2470–2486 (2018).
64. Flavin, W. P. et al. Endocytic vesicle rupture is a conserved mechanism of cellular invasion by amyloid proteins. *Acta Neuropathol.* **134**, 629–653 (2017).
65. Renier, N. et al. iDISCO: a simple, rapid method to immunolabel large tissue samples for volume imaging. *Cell* **159**, 896–910 (2014).
66. Song, H. et al. Targeting Gpr52 lowers mutant HTT levels and rescues Huntington's disease-associated phenotypes. *Brain* **141**, 1782–1798 (2018).
67. Li, Z. et al. Allele-selective lowering of mutant HTT protein by HTT–LC3 linker compounds. *Nature* **575**, 203–209 (2019).
68. Khaing, Z. Z. et al. Assessing forelimb function after unilateral cervical spinal cord injury: novel forelimb tasks predict lesion severity and recovery. *J. Neurotrauma* **29**, 488–498 (2012).
69. Anderson, K. D., Abdul, M. & Steward, O. Quantitative assessment of deficits and recovery of forelimb motor function after cervical spinal cord injury in mice. *Exp. Neurol.* **190**, 184–191 (2004).
70. Kawashita, E. et al. Altered behavior in mice with deletion of the alpha2-antiplasmin gene. *PLoS ONE* **9**, e97947 (2014).
71. Gonçalves, F. M. et al. Glutamatergic system and mTOR-signaling pathway participate in the antidepressant-like effect of inosine in the tail suspension test. *J. Neural Transm. (Vienna)* **124**, 1227–1237 (2017).
72. Matsuura, K., Kabuto, H., Makino, H. & Ogawa, N. Pole test is a useful method for evaluating the mouse movement disorder caused by striatal dopamine depletion. *J. Neurosci. Methods* **73**, 45–48 (1997).
73. Toledo, J. B. et al. A platform for discovery: the University of Pennsylvania integrated neurodegenerative disease biobank. *Alzheimers Dement.* **10**, 477–484 (2014).
74. Lucas, J. A. et al. Normative data for the Mattis Dementia Rating Scale. *J. Clin. Exp. Neuropsychol.* **20**, 536–547 (1998).
75. Pigott, K. et al. Longitudinal study of normal cognition in Parkinson disease. *Neurology* **85**, 1276–1282 (2015).
76. Van Deerlin, V. M. et al. Common variants at 7p21 are associated with frontotemporal lobar degeneration with TDP-43 inclusions. *Nat. Genet.* **42**, 234–239 (2010).
77. Mata, I. F. et al. GBA variants are associated with a distinct pattern of cognitive deficits in Parkinson's disease. *Mov. Disord.* **31**, 95–102 (2016).
78. Laird, N. M. & Ware, J. H. Random-effects models for longitudinal data. *Biometrics* **38**, 963–974 (1982).
79. Lee, R. S. et al. Relative expression levels rather than specific activity plays the major role in determining in vivo AKT isoform substrate specificity. *Enzyme Res.* **2011**, 720985 (2011).
80. Chu, N. et al. Akt kinase activation mechanisms revealed using protein semisynthesis. *Cell* **174**, 897–907 (2018).
81. Franke, T. F. et al. The protein kinase encoded by the Akt proto-oncogene is a target of the PDGF-activated phosphatidylinositol 3-kinase. *Cell* **81**, 727–736 (1995).
82. Carpten, J. D. et al. A transforming mutation in the pleckstrin homology domain of AKT1 in cancer. *Nature* **448**, 439–444 (2007).
83. Parikh, C. et al. Disruption of PH-kinase domain interactions leads to oncogenic activation of AKT in human cancers. *Proc. Natl Acad. Sci. USA* **109**, 19368–19373 (2012).
84. Langston, J. W. The MPTP story. *J. Parkinsons Dis.* **7**, S11–S19 (2017).
85. Choi, W. S., Kruse, S. E., Palmiter, R. D. & Xia, Z. Mitochondrial complex I inhibition is not required for dopaminergic neuron death induced by rotenone, MPP^+, or paraquat. *Proc. Natl Acad. Sci. USA* **105**, 15136–15141 (2008).
86. Sanchez-Ramos, J. R., Michel, P., Weiner, W. J. & Hefti, F. Selective destruction of cultured dopaminergic neurons from fetal rat mesencephalon by 1-methyl-4-phenylpyridinium: cytochemical and morphological evidence. *J. Neurochem.* **50**, 1934–1944 (1988).
87. Cohen, E. & Dillin, A. The insulin paradox: aging, proteotoxicity and neurodegeneration. *Nat. Rev. Neurosci.* **9**, 759–767 (2008).

Acknowledgements The work was supported in part by NIH grants 1 R01 GM133172 and 1 R01 HL147379 (to D.R.), NS088322 (to K.C.L.), and R01 NS115139, P50 NS053488 and U19-AG062418 (to A.S.C.-P.). A.S.C.-P. is also supported by the Parker Family Chair. B.L. is supported in part by the National Natural Science Foundation of China (81925012) and the Newton Advanced Fellowship (NAF_R1_191045). We thank the Transgenic and Chimeric Mouse Core of the University of Pennsylvania for the generation of all transgenic lines (supported by NIH centre grants P30DK050306, P30DK019525, and P30CA016520); A. Caputo for help with preparing the preformed α-syn fibrils; T. O'Brien for discussion on behavioural studies; and D. Weintraub, V. Van Deerlin and J. Trojanowski for help with human cohort studies. Some data used in the preparation of this Article were obtained from the PPMI database (www.ppmi-info.org/data). PPMI—a public–private partnership—is funded by the Michael J. Fox Foundation for Parkinson's Research and funding partners, including Abbvie, Allergan, Amathus therapeutics, Avid Radiopharmaceuticals, Biogen, BioLegend, Bristol–Myers Squibb, Celgene, Denali, GE Healthcare, Genentech, GlaxoSmithKline, Golub Capital, Handl Therapeutics, Insitro, Janssen Neuroscience, Lilly, Lundbeck, Merck, Meso Scale Discovery, Pfizer, Piramal, Prevail Therapeutics, Roche, Sanofi Genzyme, Servier, Takeda, Teva, UCB, Verily and Voyager Therapeutics. Up-to-date information on the study is available at www.ppmi-info.org.

Author contributions J.W. performed all the electrophysiology studies, the neuronal damage analysis, the α-syn PFF seeding assay, galectin 3 assay, BODIPY–pepstatin A assay, autophagosome fusion assay and pH imaging in Fig. 5a and Extended Data Figs. 8–10. Z.L. and J.W. carried out the protein chemistry, RT–PCR analysis and S2 cell Akt knockdown studies. K.A., J.L. and D.R. developed cDNA constructs and mouse lines. C.C. performed earlier exploratory recordings that demonstrated that the TMEM175-knockout lysosomes lack TMEM175 currents and that SC79 activates TMEM175. Y.L. and K.C.L. performed TH immunostaining comparing the wild-type and homozygous mouse brains, and prepared and validated the α-syn PFFs. L.Y., H.W. and J.Y. performed the whole-tissue immunolabelling, optical clearing and light-sheet 3D imaging analysis comparing the wild-type and heterozygous mouse brains. H.S. and B.L. performed the mouse behavioural studies. T.F.T. and A.S.C.-P. carried out the clinical studies. D.R., J.W., B.L., J.Y., A.S.C.-P. and K.C.L. designed experiments and wrote the manuscript with contributions from all the authors.

Competing interests The authors declare no competing interests.

Additional information

Supplementary information The online version contains supplementary material available at https://doi.org/10.1038/s41586-021-03185-z.

Correspondence and requests for materials should be addressed to A.S.C.-P., K.C.L. or D.R.

Peer review information *Nature* thanks David Stone and the other, anonymous, reviewer(s) for their contribution to the peer review of this work.

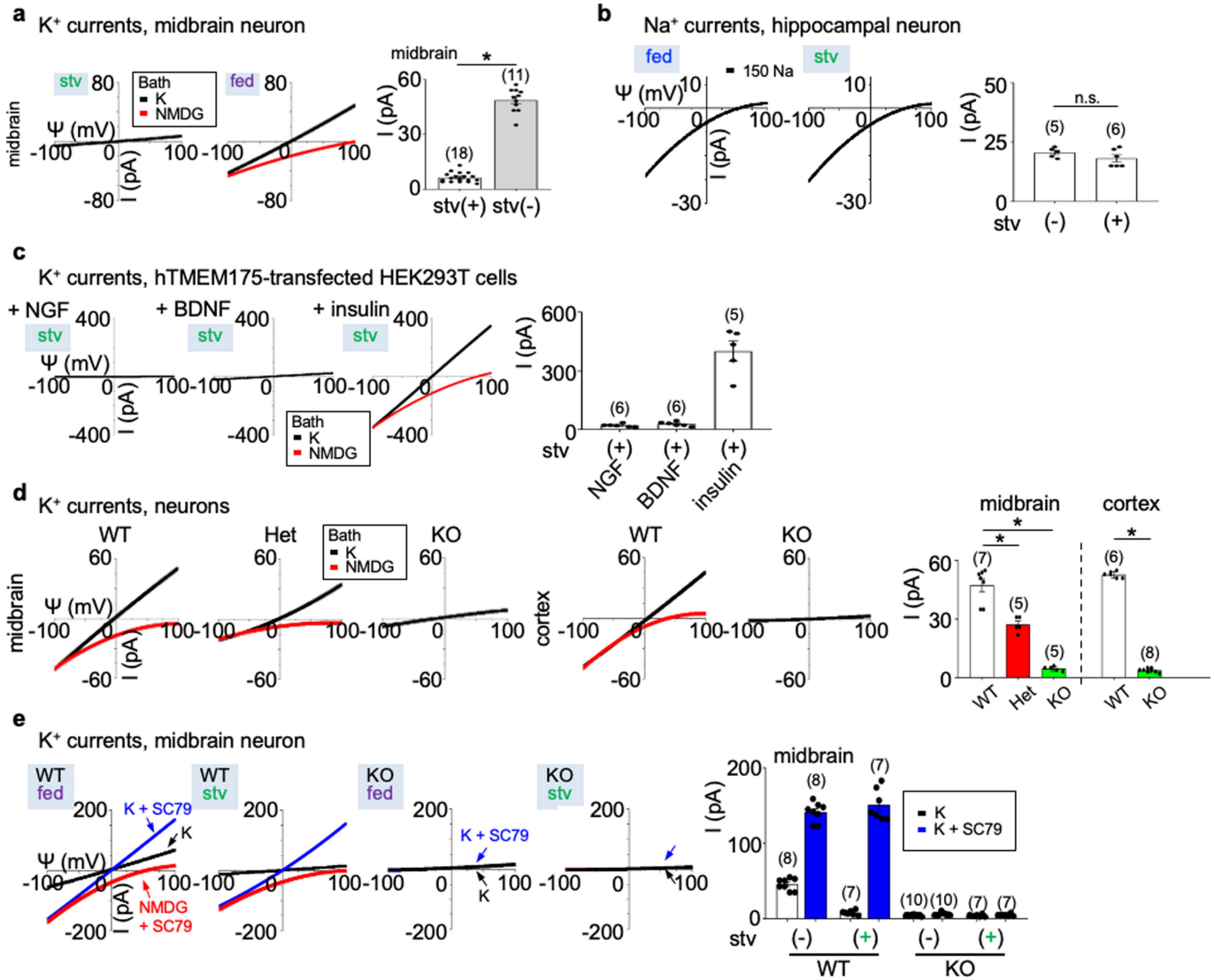

Extended Data Fig. 1 | Lysosomal currents activated by growth factors. Lysosomal currents were recorded using a ramp protocol (−100 mV to 100 mV ramp in 1 s with holding voltage of 0 mV) as illustrated in Fig. 1. **a**, Sizes of K^+ currents (I_K) recorded at varying voltages (Ψ, −100 mV to 100 mV) from midbrain neurons with (stv) or without (fed) overnight starvation in DMEM containing no B27 nutrient supplement. Averaged I_K sizes (at 100 mV, recorded with 150 mM K^+-containing bath) are in the right bar graph. Data are mean ± s.e.m. Numbers of recordings are in parentheses. *$P < 0.0001$, unpaired two-tailed *t*-test. **b**, Na^+ currents recorded from hippocampal neurons with and without starvation demonstrating that B27 does not activate Na^+ currents. The averaged current sizes (at −100 mV) are in the right bar graph ($P = 0.226$, unpaired two-tailed *t*-test). Solutions used in the recordings were the same as those used to record the I_K in Fig. 1a, b, except that K^+ in the bath was replaced with Na^+ and 1 μM $PI(3,5)P_2$ was added in the bath (lysosomal Na^+ channel requires $PI(3,5)P_2$ for maximum activation). **c**, I_K recorded from TMEM175-transfected HEK293T cells starved in HBSS followed by refeeding with NGF (100 ng ml^{-1} for 3 h) or BDNF (10 ng ml^{-1} for 3 h), demonstrating that BDNF and NGF do not activate TMEM175 in HEK293T cells. Activation by insulin (right) was used as a positive control for receptor activation (see Fig. 1f for insulin). Averaged I_K sizes (recorded with K^+-containing bath, at 100 mV) are in the right bar graph. **d**, I_K recorded from B27-replete midbrain and cortical neurons cultured from wild-type, heterozygous or TMEM175-knockout mice. Averaged I_K sizes (at 100 mV, recorded with 150 mM K^+-containing bath) are in the right bar graph. Data are mean ± s.e.m. Numbers of recordings are in parentheses. *$P < 0.001$, unpaired two-tailed *t*-test. *P* values (compared to wild type) are as follows: midbrain, $P = 0.0007$ for heterozygous, $P < 0.0001$ for knockout; cortex, $P < 0.0001$ for knockout. **e**, I_K recorded from wild-type and TMEM175-knockout midbrain neurons before (fed) or after (stv) starvation (overnight in DMEM). An AKT activator SC79 (10 μM) was applied to the recording bath during some of the recordings (blue and red traces). Bar graphs in the right show averaged I_K sizes (at 100 mV). Data are mean ± s.e.m. Numbers of recordings are in parentheses. Arrows are used to indicate curves that overlap and are not easily distinguished.

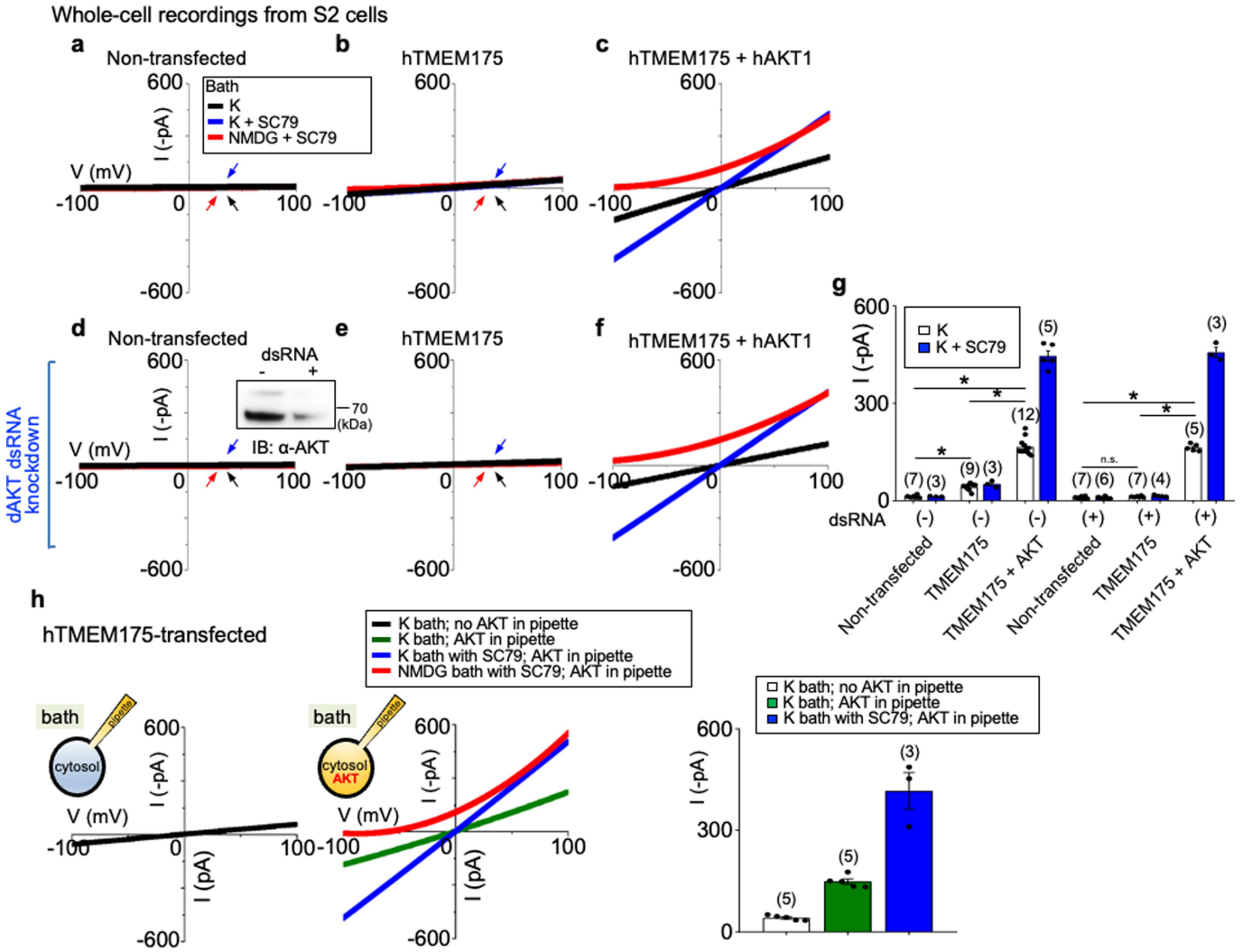

Extended Data Fig. 2 | AKT is required for the reconstitution of human TMEM175 as a functional ion channel. a–**f**, Whole-cell currents were recorded from *Drosophila* S2 cells without (**a**–**c**, **h**) or with (**d**–**f**) endogenous Akt ('dAKT') knocked down using dsRNA treatment. **a**, **d**, Nontransfected S2 cells. **b**, **e**, **h**, S2 cells transfected with human TMEM175 alone. **c**, **f**, S2 cells cotransfected with human TMEM175 and human AKT1. A western blot showing the reduction of *Drosophila* Akt protein by dsRNA treatment is shown in the inset in **d**. For gel source data, see Supplementary Fig. 1. **g**, Summary of current amplitudes (at −100 mV, recorded in K^+-containing bath with or without SC79). Recordings were done using a ramp protocol (−100 mV to 100 mV in 1 s, V_h = 0 mV). Bath solution contained 150 mM K^+, 150 mM K^+ with SC79 (an activator of human AKT) or 150 mM NMDG with SC79, as indicated. In **a**, **b**, **d**, **e**, arrows are used to indicate curves that overlap and are not easily distinguished. Black, recorded from bath containing K^+; blue, recorded from bath containing K^+ and SC79; red, recorded from bath containing NMDG and SC79. Data are mean ± s.e.m. Numbers of recordings are in parentheses. In **g**, *$P \leq 0.05$ (compared with those from cells cotransfected with human TMEM175 and human AKT). *P* values (unpaired two-tailed *t*-tests) are as follows: without dsRNA treatment, $P < 0.0001$ for TMEM175 vs nontransfected, TMEM175+AKT vs nontransfected and TMEM175+AKT vs TMEM175; with dsRNA treatment, $P = 0.1253$ for TMEM175 vs nontransfected, $P < 0.0001$ for TMEM175+AKT vs TMEM175 and TMEM175+AKT vs nontransfected. **h**, Whole-cell currents recorded from S2 cells transfected with human TMEM175 alone, with (middle) or without (left) recombinant human AKT1 protein (1 μg ml^{-1}) included in the pipette solution. Right, summary of current amplitudes (at −100 mV; **b** and **g** show an additional control without AKT protein in pipette. We further tested the necessary and sufficient role for AKT in $I_{TMEM175}$ by reconstituting TMEM175 in the *Drosophila* S2 cell line, which does not have endogenous TMEM175. In HEK293T cells, cotransfection of AKT1 did not further increase $I_{TMEM175}$ (Extended Data Fig. 6a), consistent with the idea that the three mammalian AKTs are already abundantly expressed in the cells[79]. S2 cells do not have *TMEM175* (which is absent in insects), and have only one *Akt* gene, making it easier to knock down. In addition, the *Drosophila* Akt (dAKT) protein is not well-conserved with the mammalian AKTs (61% identity to human AKT1) and is less likely to support human TMEM175 function. For technical reasons, we were unable to enlarge S2 cell lysosomes suitable for patch-clamp recording. We therefore recorded whole-cell currents as an assay for functional channels. Transfecting human TMEM175 alone into S2 cells generated little current (about −20 pA at −100 mV) above the level of endogenous K^+ currents (**a**, **b**, **g**). In addition, knocking down *Drosophila Akt* with dsRNA[55] completely eliminated the small $I_{TMEM175}$ (**d**, **e**, **g**). Cotransfecting human TMEM175 with a human AKT1 (hAKT1), however, led to robust $I_{TMEM175}$, either with or without the endogenous *Drosophila Akt* knocked down (**c**, **f**, **g**). The currents were potentiated by SC79 in human AKT cotransfected cells but not in those transfected with TMEM175 alone, supporting the notion that SC79 acts on mammalian AKTs to open the channel. We finally tested whether purified recombinant AKT protein is sufficient to activate TMEM175. In S2 cells transfected with human TMEM175 alone (which had minimal current), application of SC79 into the bath increased the currents to −417.0 ± 53.9 pA (**h**) (n = 3, −100 mV) when human AKT1 protein was introduced into cytosol via pipette solution dialysis. Together, our data suggest that AKT is obligatory for a functional mammalian TMEM175 channel.

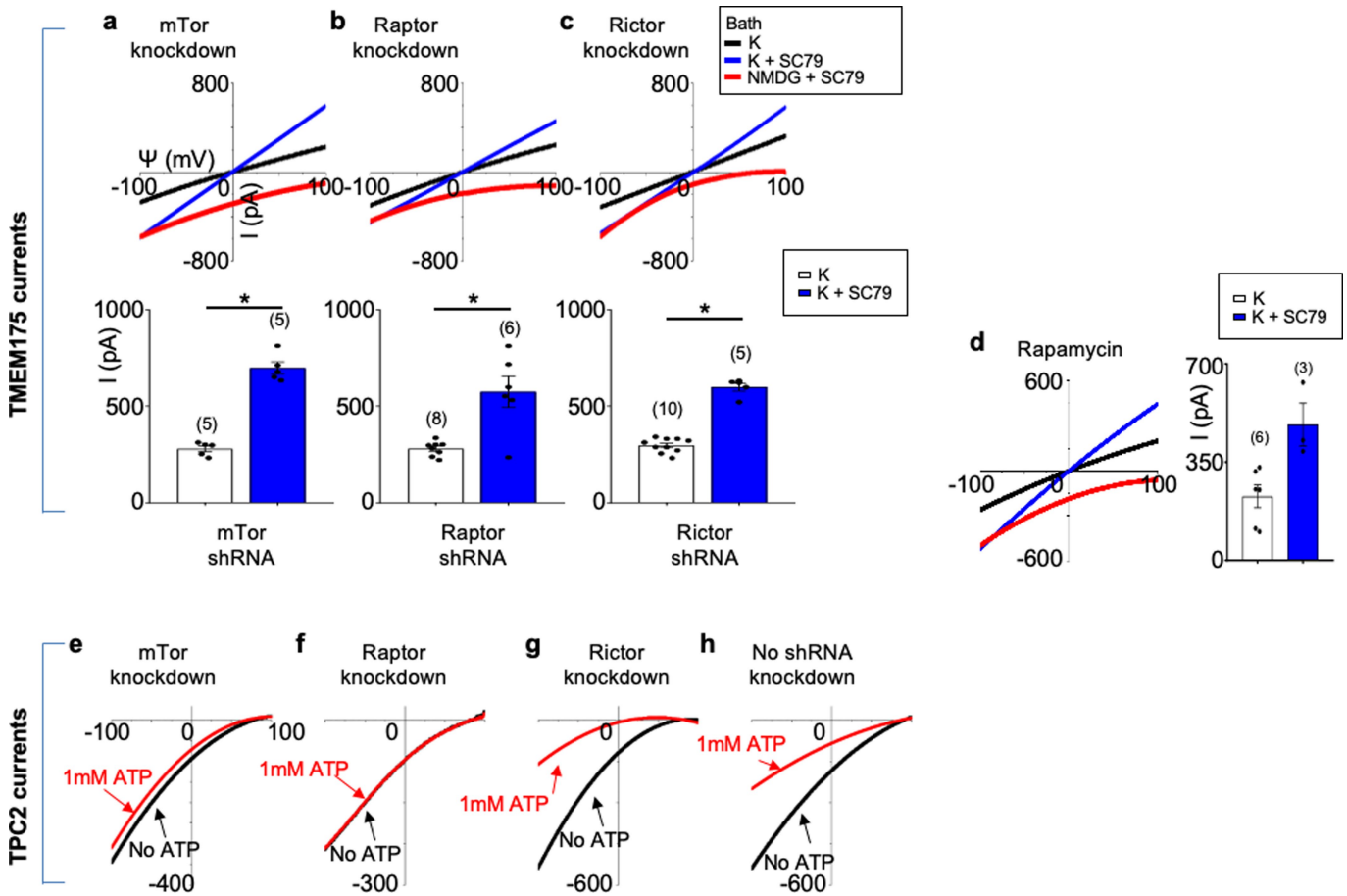

Extended Data Fig. 3 | mTOR is not required for the activation of TMEM175 by AKT. a–**c**, Lysosomal I_K currents were recorded from TMEM175-tranfected HEK293T cells with mTOR (a component of both mTORC1 and mTORC2 complexes) (**a**), Raptor (an mTORC1 component) (**b**) or Rictor (an mTORC2 component) (**c**) knocked down with short hairpin (sh)RNA lentivirus[10]. **d**, Lysosomal I_K recorded from TMEM175-tranfected HEK293T cells treated with rapamycin (2 μM, 1 h). Figure 1f provides comparisons with those with no knockdown or rapamycin treatment. *$P \leq 0.05$. P values (unpaired two-tailed t-tests; K vs K+SC79 groups) are: $P < 0.0001$ (mTor shRNA), $P = 0.0013$ (Raptor shRNA), $P < 0.0001$ (Rictor shRNA). **e**–**h**, Control for mTOR knockdown. Lysosomal Na^+ currents were recorded from HEK293T cells transfected with TPC2 as positive controls for mTOR knockdown. TPC2 is a lysosomal Na^+ channel that is inhibited by ATP. The ATP sensitivity requires mTORC1 but not mTORC2; knocking down mTOR or Raptor—but not Rictor—reduces the ATP sensitivity[10]. In **f**, arrows are used to indicate traces that overlap and are not easily distinguished. Black, recorded before 1 mM ATP was added to the bath; red, recorded after 1 mM ATP was added to the bath. Data are mean ± s.e.m. Numbers of recordings are in parentheses.

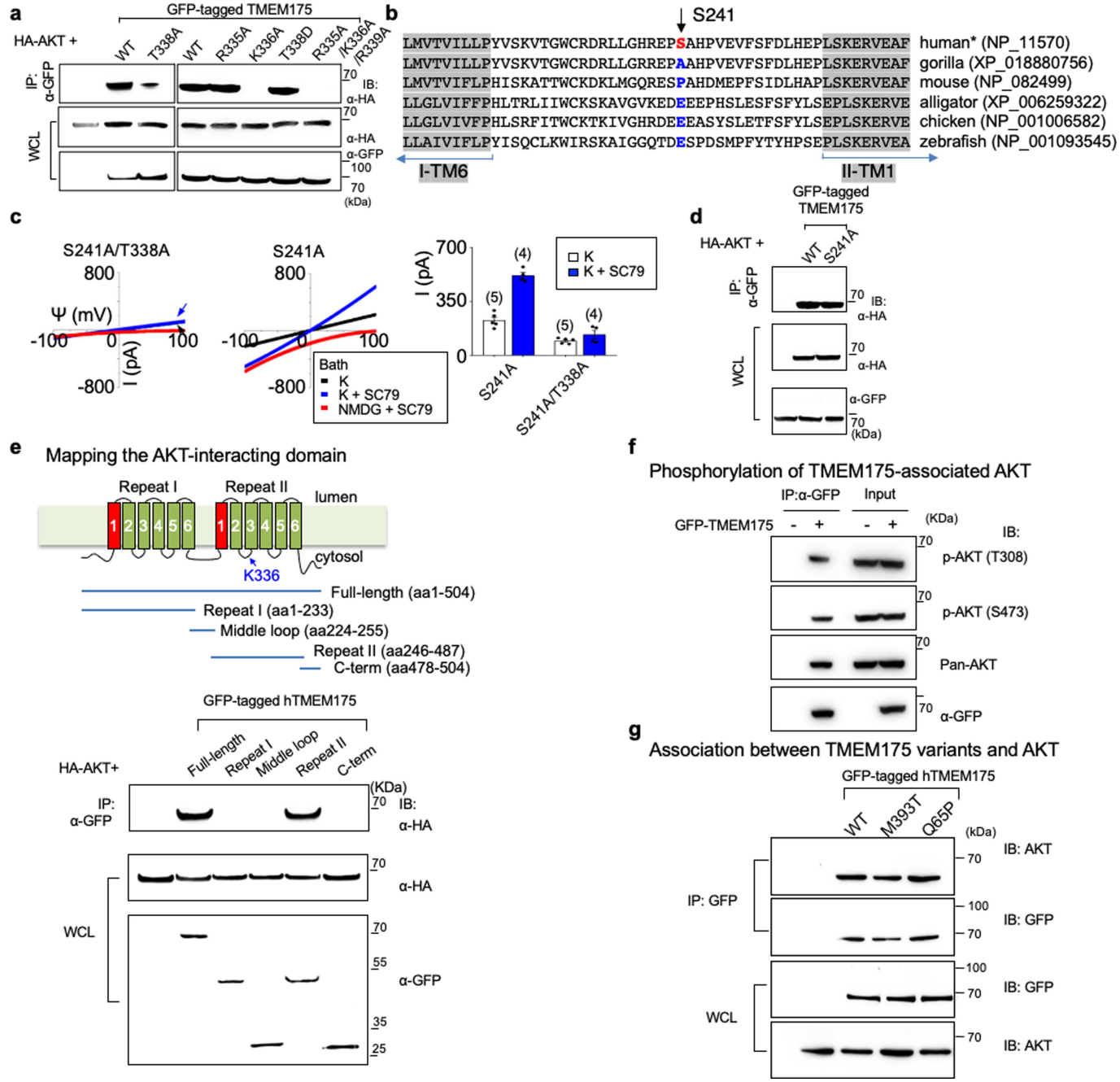

Extended Data Fig. 4 | Characterization of TMEM175–AKT interaction and its role in TMEM175 activation. a, Association between heterologously expressed TMEM175 and AKT. HEK293T cells were transfected with GFP-tagged wild-type or mutant TMEM175 and HA-tagged human AKT1 (HA–AKT), as indicated. Lysates were immunoprecipitated with anti-GFP and blotted with anti-GFP or with anti-AKT. Whole-cell lysate was also blotted for input control. **b**–**d**, Experiments demonstrating that S241 is not essential for TMEM175 activation. **b**, Sequence alignment of the region around S241 of TMEM175. GenBank access numbers are in parentheses. **c**, Lysosomal I_K recorded from HEK293T cells transfected with S241A/T338A or S241A substitutions. Averaged I_K sizes (at 100 mV) are shown in the bar graphs. Data are mean ± s.e.m. Numbers of lysosomes recorded are in parentheses. **d**, Association between wild-type or S241A-mutant TMEM175 and AKT. HA-tagged AKT was transfected alone (lane 1) in HEK293T cells or together with GFP-tagged wild-type or S241A-mutant human TMEM175 (lanes 2 and 3). Whole-cell lysates were blotted with anti-GFP (bottom) or anti-HA (middle), or immunoprecipitated with anti-GFP followed by immunoblotting with anti-HA (top). In **c**, arrows are used to indicate curves that overlap and are not easily distinguished. Black, recorded from bath containing K^+; blue, recorded from bath containing K^+ and SC79. **e**, Mapping the AKT-interacting region to the second repeat of TMEM175. A diagram illustrating the GFP-tagged TMEM175 fragments used in the experiments is shown. Lysates from HEK293T cells transfected with HA-tagged AKT1 (HA–AKT) alone (lane 1) or together with GFP-tagged TMEM175 fragments (lanes 2–6) were blotted with anti-GFP (bottom) or anti-HA (middle) or immunoprecipitated with anti-GFP followed by blotting with anti-HA (top). **f**, Phosphorylation status of T308 and S473 of TMEM175-associated AKT. HEK293T cells were transfected with GFP-tagged TMEM175 (with nontransfected cells as control). Endogenous AKT associated with TMEM175 was pulled down with immunoprecipitation using anti-GFP and was probed with antibodies against total AKT (pan-AKT), AKT phosphorylated at T308 (pAKT(T308)) or at S473 (pAKT(S473)). Total cell lysates (input) before immunoprecipitation were also loaded for comparison. **g**, Association between TMEM175(M393T) and TMEM175(Q65P) and AKT. Lysates from HEK293T cells transfected with GFP-tagged wild-type or mutant TMEM175 (with nontransfected cells as control) were blotted with anti-GFP, anti-AKT or immunoprecipitated with anti-GFP followed by blotting with anti-GFP or anti-AKT. For gel source data, see Supplementary Fig. 1.

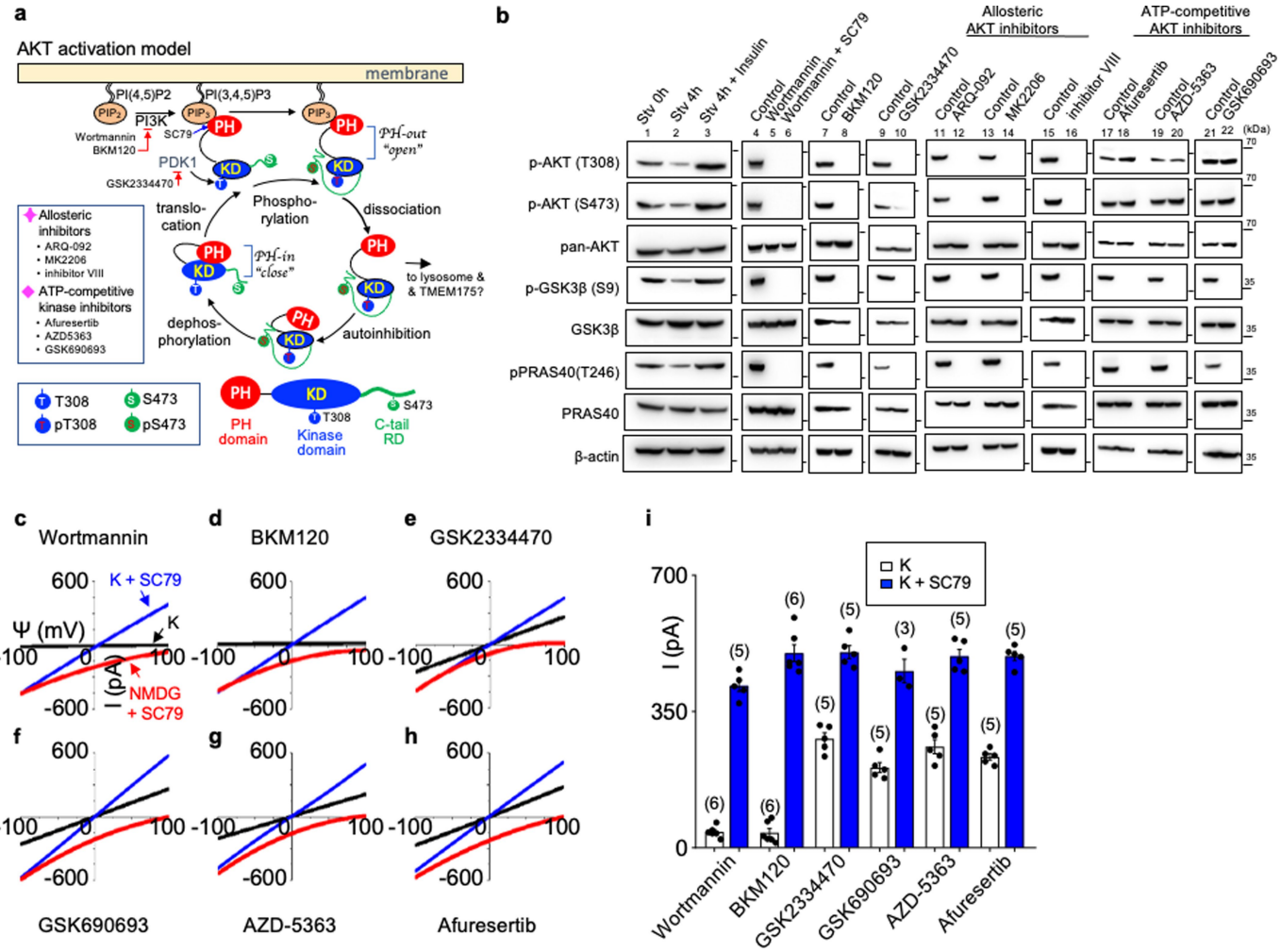

Extended Data Fig. 5 | See next page for caption.

Extended Data Fig. 5 | AKT activates TMEM175 in a catalytic activity-independent manner. a, Schematic of the canonical AKT activation, with inhibitors used to target each step indicated, modified from previous publications[23,80]. A domain structure of AKT is in the bottom. AKT has a PH domain (PH), a kinase domain (KD) and a C-terminal tail regulatory domain (RD). **b**, Phosphorylation status of AKT and its two canonical targets GSK3β and PRAS40 following treatments similar to those used in the patch-clamp recording of TMEM175. Lysates from human TMEM175-transfected cells were probed with antibodies as indicated. Treatment conditions were: starvation (0 h, 4 h in HBSS) without (lanes 1 and 2) or with insulin (lane 3, 100 nM, 4 h) treatment afterwards, wortmannin (20 μM, 2 h) with and without SC79 (10 μM, 30 min) treatment afterwards (lanes 5 and 6), BKM120 (10 μM, 3 h; lane 8), GSK2334470 (20 μM, 3 h; lane 10), ARQ-092 (20 μM, 3 h; lane 12), MK2206 (20 μM, 3 h; lane 14), inhibitor VIII (10 μM, 3 h; lane 16), afuresertib (20 μM, 3 h; lane 18), AZD-5363 (20 μM, 3 h; lane 20), GSK690693 (10 μM, 4 h; lane 22). For gel source data, see Supplementary Fig. 1. **c**–**i**, Lysosomal I_K was recorded from TMEM175-transfected HEK293T cells pretreated with wortmannin (**c**), BKM120 (**d**), GSK2334470 (**e**), GSK690693 (**f**), AZD-5363 (**g**) or afluresertib (**h**) as in **b** before lysosomal dissection for recording. Averaged I_K sizes (at 100 mV) are shown in **i**. Data are mean ± s.e.m. Numbers of recordings are in parentheses. Our finding that SC79 fully activates TMEM175 in starved lysosomes was surprising but is also consistent with the idea that channel activation is independent of the kinase activity of AKT. Upon receptor activation by growth factors, PI3 kinases (PI3Ks) increase the concentration of PIP_3 from PtdIns(4,5)P_2 (PIP_2)[18]. SC79 and the endogenous AKT activator PIP_3 both bind to the PH domain of AKTs to induce large conformational changes that lead to the release of the PH domain from the catalytic domain and to an open state of the kinase[19], which renders AKT accessible to phosphorylation at a key residue in the kinase domain (T308 in human AKT1) by PKD1 and another residue (S473) in the C-terminal regulatory domain by kinases such as mTORC2. Phosphorylation of T308 and S473 is required for the efficient activation of AKT kinase activity to phosphorylate downstream targets such as GSK3β and PRAS40[18] (**a**). In nutrient-replete cells, TMEM175-associated AKT is at least partially phosphorylated at the two sites (Extended Data Fig. 4f). We used a panel of AKT inhibitors and mutants to probe the involvement of each of the steps in AKT function in TMEM175 activation. In starved cells and wortmannin-treated ones, AKT kinase activity is minimal because of the lack of phosphorylation of T308 on AKT by PKD1. Indeed, the activation of AKT kinase activity by SC79 on AKT isolated from starved cells requires the addition of PKD1 and ATP. Similarly, SC79 does not induce substantial AKT kinase activity (assayed with target phosphorylation) in wortmannin-treated cells[19] (**b**). However, SC79 maximally activated TMEM175 in lysosomes isolated from starved cells (Fig. 2d, h) and in those from wortmannin-treated cells (**c**, **i**), without PKD1 or ATP in the bath, supporting that the SC79-induced channel activation does not require the kinase activity of AKT. Reduction of PIP_3 by starvation and by inhibition of PI3K with wortmannin or BKM120 (a specific PI3K inhibitor)—treatments expected to keep AKT in a PH-in a closed state—both reduced the phosphorylation of AKT at T308 and S473 and that of the downstream AKT targets GSK3 (S9) and PRAS40 (T246) (**b**). The treatments also eliminated $I_{TMEM175}$, which was restored by SC79 application (**b**–**d**, **i**). These data suggest that AKT activates channel after it switches from the PH-in closed state to the PH-out open state. To further test whether—after AKT switches to a PH-out open state—phosphorylation of T308 in AKT by PDK1 is required for $I_{TMEM175}$, we inhibited PDK1 with GSK2334470. Although the inhibitor abolished the phosphorylation of AKT and its downstream targets, it had little effect on $I_{TMEM175}$ (**b**, **e**, **i**). Catalytic and allosteric AKT inhibitors both block phosphorylation of downstream targets by AKT, but via different mechanisms[18] (**a**). Unlike allosteric inhibitors, which probably keep AKT in a closed phosphorylation-resistant state and prevent the activation of TMEM175 (**b**, Fig. 2f), catalytic inhibitors such as those that compete with ATP binding in the activation loop are downstream of the phosphorylation of AKT T308 and S473 and inhibit AKT kinase activities in an open state. The ATP competitive inhibitors GSK690693, AZD-5363 and GSK2110183 (afuresertib) all inhibited AKT target phosphorylation (**b**), but—in contrast to the allosteric inhibitors (Fig. 2f)—had little effect on $I_{TMEM175}$ (**f**–**i**). Together, the inhibitors targeting different steps of AKT activation suggest that conformational changes that lead to AKT in an open state, but not the downstream steps of the catalytic activities of AKT, are required for $I_{TMEM175}$.

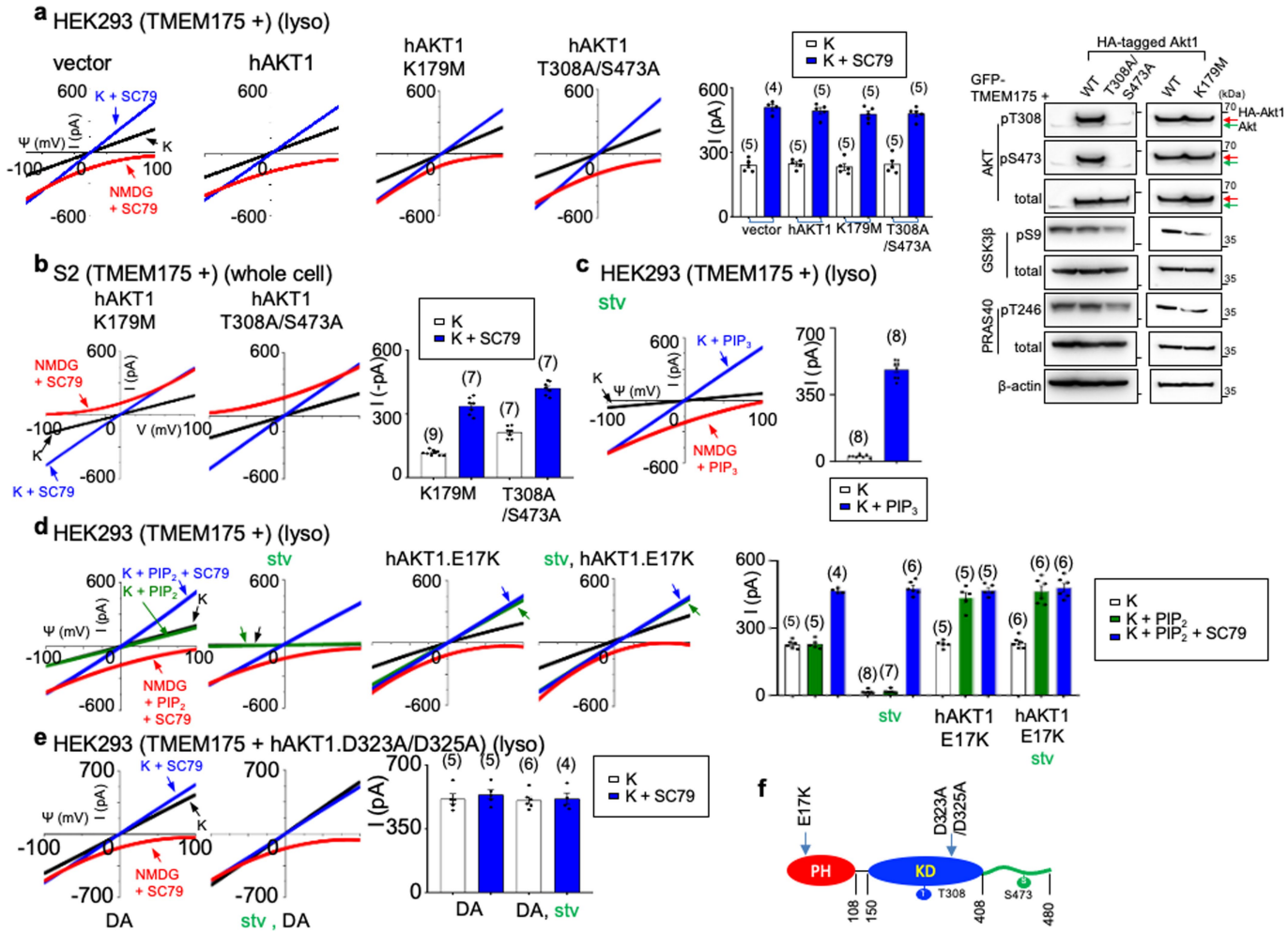

Extended Data Fig. 6 | AKT determines the sensitivity of TMEM175 to starvation and activation by phosphatidylinositol lipids. a–**e**, HEK293T cells (**a**, **c**–**e**) (lysosomal recording) or S2 cells (**b**) (whole-cell recording) were transfected with human TMEM175 with or without cotransfection of wild-type or mutant human AKT1. **a**, **b**, Experiments demonstrating that AKT with mutations in the kinase domain (K179M alone, T308A/S473A double mutant) are able to support $I_{TMEM175}$ as well as wild-type AKT. Extended Data Figure 2 provides a comparison with those from S2 cells transfected with TMEM175 without human AKT1 cotransfection, in which very little currents were generated. A summary of current amplitudes (at −100 mV) is given in the bar graphs. The right panel in **a** shows the phosphorylation status of transfected AKT and AKT targets GSK3β and PRAS40. The human AKT1 used for transfection has an HA tag and a linker sequence, and can be distinguished from the endogenous AKT (indicated by green arrows) because of its slightly higher molecular weight. For gel source data, see Supplementary Fig. 1. In **c**–**e**, stv indicates cells starved in HBSS medium for 2 h before lysosomal dissection for recording. **c**, PIP_3 (1 μM) was applied to the recording bath during some of the recordings (blue and red traces). **d**, **e**, $I_{TMEM175}$ recorded from lysosomes with or without cotransfection of the E17K (**d**) or the D323A/D325A (DA) (**e**) AKT1 mutants, with or without starvation. PIP_2 in **d** was applied at 1 μM. Data are mean ± s.e.m. Numbers of recordings are in parentheses. Arrows are used to indicate curves that overlap and are not easily distinguished. **f**, Positions of the AKT1 mutations used in this figure. We used AKT mutants to further test the nonessential role of kinase activity in $I_{TMEM175}$. AKT1 with mutation at K179 (a key residue in the ATP- and Mg^{2+}-binding pocket; K179M), or at T308 and S473 (residues key to AKT kinase activation; T308A/S473A) no longer phosphorylates its targets[18,81]. $I_{TMEM175}$ from cells co-expressing the mutants, however, was similar to that co-expressing wild-type AKT (**a**). More importantly, when co-expressed with human TMEM175 in S2 cells, the kinase-inactive mutants fully supported $I_{TMEM175}$ in a manner indistinguishable from that of the wild type (**b**). We then tested whether AKT conformational changes are sufficient to activate the channel. Under physiological conditions, PIP_3 generated on the plasma membrane opens AKT by binding to the PH domain. In lysosomes from starved cells, PIP_3 bath application activated $I_{TMEM175}$ (**c**). The E17K mutation in the PH domain—commonly found in cancers—switches the lipid sensitivity of AKT from PIP_3 to PIP_2, a lipid that is abundant even during starvation[82]. Notably, $I_{TMEM175}$ from cells cotransfected with AKT(E17K) was resistant to starvation, and, unlike that without cotransfection, was activated by PIP_2 (**d**). Thus, AKT also determines the lipid sensitivity of TMEM175. The double mutation D323A/D325A of AKT1 disrupts the locking of the PH domain to the kinase domain and keeps AKT in a constitutively open state[23,83]. $I_{TMEM175}$ from cells co-expressing this mutant was resistant to starvation, maximally activated and not further activated by SC79 (**e**).

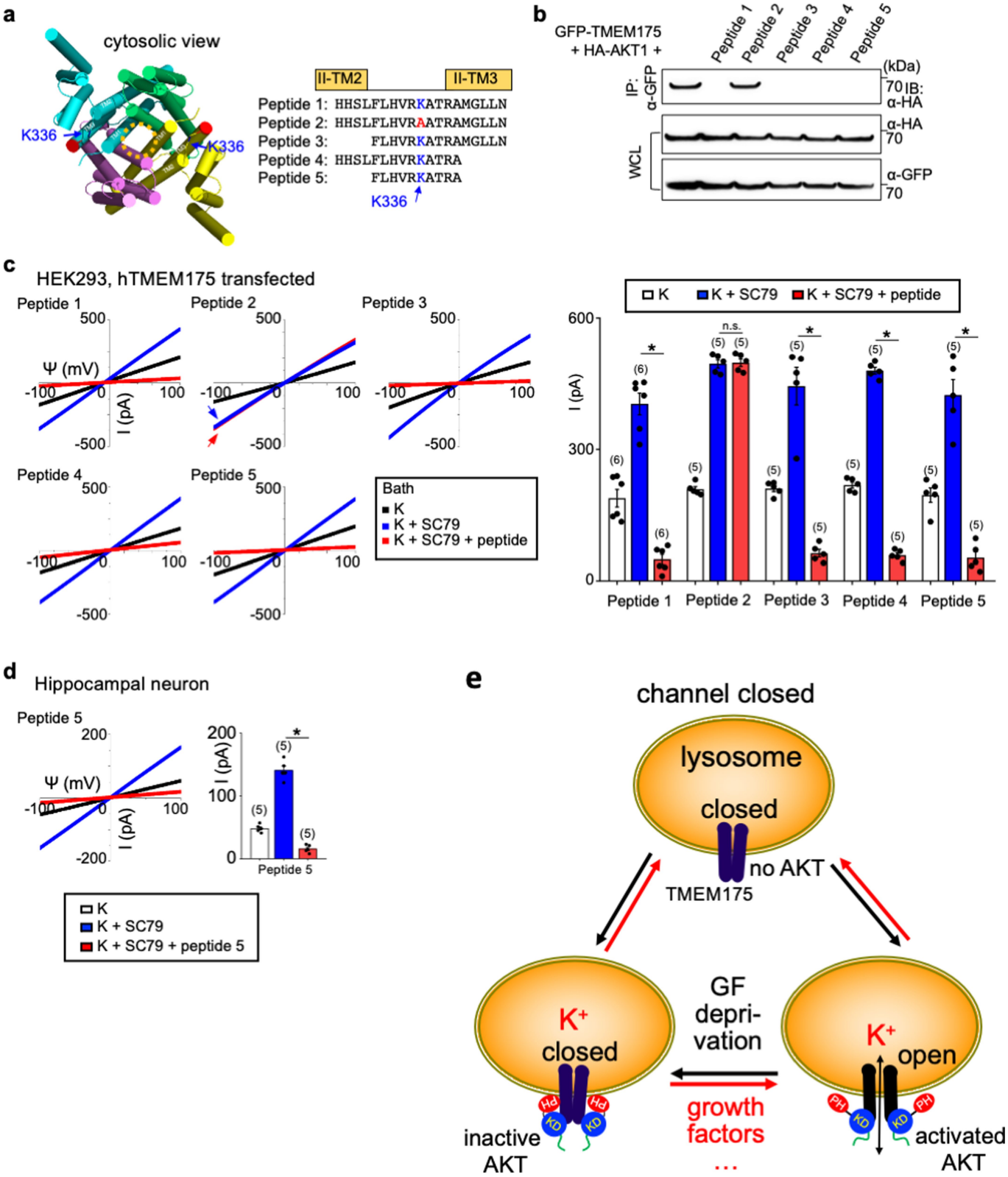

Extended Data Fig. 7 | See next page for caption.

Extended Data Fig. 7 | Association of AKT to TMEM175 is required to maintain $I_{TMEM175}$ after the channel is activated. a, **b**, Development of peptide inhibitors that dissociate AKT from TMEM175 in the lysoK$_{GF}$ complex. **a**, Sequences of synthesized human TMEM175 peptides around the K336 region that interacts with AKT. Peptide 2 has a K336A mutation. **b**, To test the ability of each peptide to dissociate AKT from TMEM175, cell lysates from HEK293T cells cotransfected with GFP-tagged human TMEM175 and HA-tagged human AKT1 were incubated with each peptide (10 μM) for 2 h before immunoprecipitation with anti-GFP to bring down TMEM175 and immunoblotting with anti-HA to detect the associated AKT1. Immunoprecipitation without peptide incubation (lane 1) was used as a control. Whole-cell lysate was also blotted with anti-HA and anti-GFP for input control. For gel source data, see Supplementary Fig. 1. The results show that when applied in cell lysates containing the TMEM175–AKT complex, peptides as short as 10 amino acids (peptide 5) in the K336 region were sufficient to dissociate AKT from the preassembled AKT–TMEM175 complex in the immunoprecipitation assay. As a control, K336A mutation (peptide 2) abolished the dissociation ability of the peptide. **c**, **d**, Lysosomal I_K were recorded from TMEM175-transfected HEK293T cells (**c**) and mouse hippocampal neurons (**d**). After SC79 application to maximally activate lysoK$_{GF}$, peptide inhibitor (10 μM) was added to the bath and currents were recorded for about 10 min until they reached steady states. The K336A mutant peptide 2 was used as a negative control. Averaged I_K sizes (at 100 mV) are shown in the bar graphs. In **c** subpanel 'peptide 2', arrows are used to indicate curves that overlap and are not easily distinguished. Blue, from bath containing K^+ and SC79 before peptide application; red, from bath containing K^+ and SC79 after peptide application. Data are mean ± s.e.m. Numbers of recordings are in parentheses. *$P \leq 0.05$. *P* values (unpaired two-tailed *t*-tests) (K+SC79 vs K+SC79 + peptide groups) are as follows. In **c**, $P = 0.8447$ for peptide 2, $P < 0.0001$ for the other treatments; in **d**, $P = 0.0011$ for peptide 5. The results show that after the channel was maximally activated by SC79, bath application of AKT-association peptide inhibitors—but not the one with the K336A point mutation—diminished both heterologously expressed $I_{TMEM175}$ in HEK293T cells and the native currents in neurons. Given that the bath contained no phosphatase, the action of the peptides is unlikely through a dephosphorylation of the channel target but is rather through the dissociation of AKT from TMEM175—further supporting the idea that it is the conformational change of AKT, and not target phosphorylation, that activates the channel. **e**, A model for TMEM175 activation by AKT conformational changes. TMEM175 without AKT or associated with inactive AKT in its PH-in closed conformation is closed. The channel opens upon AKT conformational changes triggered by physiological activators such as extracellular growth factors, lipids, or synthetic small molecules such as SC79. The gating mechanism does not require AKT kinase activity. AKT mutations found in cancers that alter the interaction between the PH and kinase domains also alter TMEM175 channel property.

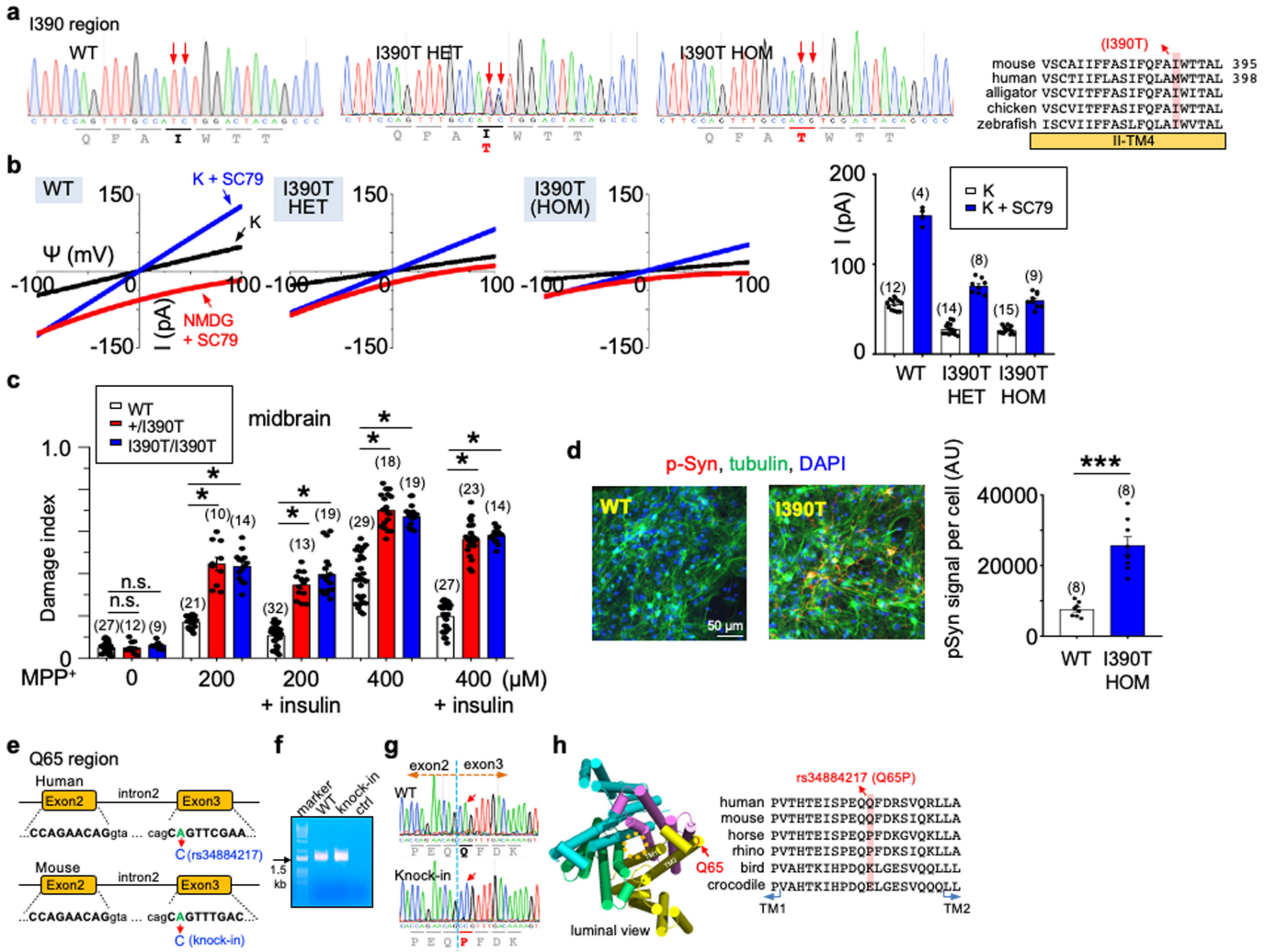

Extended Data Fig. 8 | Knock-in mice to model common human variants p.M393T and p.Q65P. a–**d**, Experiments demonstrating that the TMEM175(I390T) substitution in mice—corresponding to M393T in human TMEM175—leads to reduced lysosomal I_K, accelerated spreading of pathogenic α-syn and increased neuronal damage. **a**, Sanger sequencing of genomic DNA PCR products from wild-type, heterozygous and homozygous TMEM175(I390T) knock-in mice in the I390-coding region. Residue I390 in mouse TMEM175 is equivalent to M393 in human TMEM175, as shown in the sequence alignment on the right. **b**, I_K recorded from wild-type (+/+, wild type), heterozygous (I390T/+, het) and homozygous (I390T/I390T, hom) knock-in mouse midbrain neurons. Bar graphs show averaged I_K (at 100 mV). Data are mean ± s.e.m. Numbers of recordings are in parentheses. **c**, Neuronal damages in wild-type, het and hom midbrain neurons treated with MPP^+ with concentrations as indicated added to culture medium for 12 h and those followed by incubation with insulin (100 nM in DMEM) for 3 h. Damage index was calculated as the ratio of damaged area to the total neuronal area. **d**, Cultured wild-type and TMEM175(I390T) (hom) midbrain neurons were seeded with mouse α-syn PFFs and immunostained with anti-pSer129 α-syn (pSyn, red) two weeks later. β-Tubulin (green) was costained to highlight neuronal processes. DAPI (blue) nuclear staining was used to identify number of cells. Left two subpanels, representative images. Right, pSyn signals normalized to number of cells ($n = 8$ coverslips each). For **c**, **d**, see Fig. 5, Extended Data Fig. 10 for more details. *P* values in **c** are as follows (unpaired two-tailed *t*-tests, compared to wild type): 0 μM MPP^+, $P = 0.9318$ (het), $P = 0.2516$ (hom); $P < 0.0001$ for all the other comparisons. The *P* value in **d** (*t*-test, wild type versus hom) is $P < 0.0001$. **e**–**h**, Characterization of the rs34884217 (p.Q65P) variant. **e**, Genomic structures of the human and mouse *TMEM175* genes around the rs34884217 SNP region. The A-to-C variation in human and the corresponding substitution in the knock-in mouse line are indicated by arrows. **f**, Agarose gel electrophoresis showing RT–PCR products of the whole open reading frame cDNA (about 1.5 kb) amplified from wild-type and knock-in mouse brains. For gel source data, see Supplementary Fig. 1. **g**, Sanger sequencing results of the RT–PCR products in **f**, demonstrating that the A-to-C substitution in mice leads to a Q65P coding change. **h**, Sequence alignments around Q65 in the I-TM1–TM2 linker. Q65P is located at the luminal side of the channel entrance.

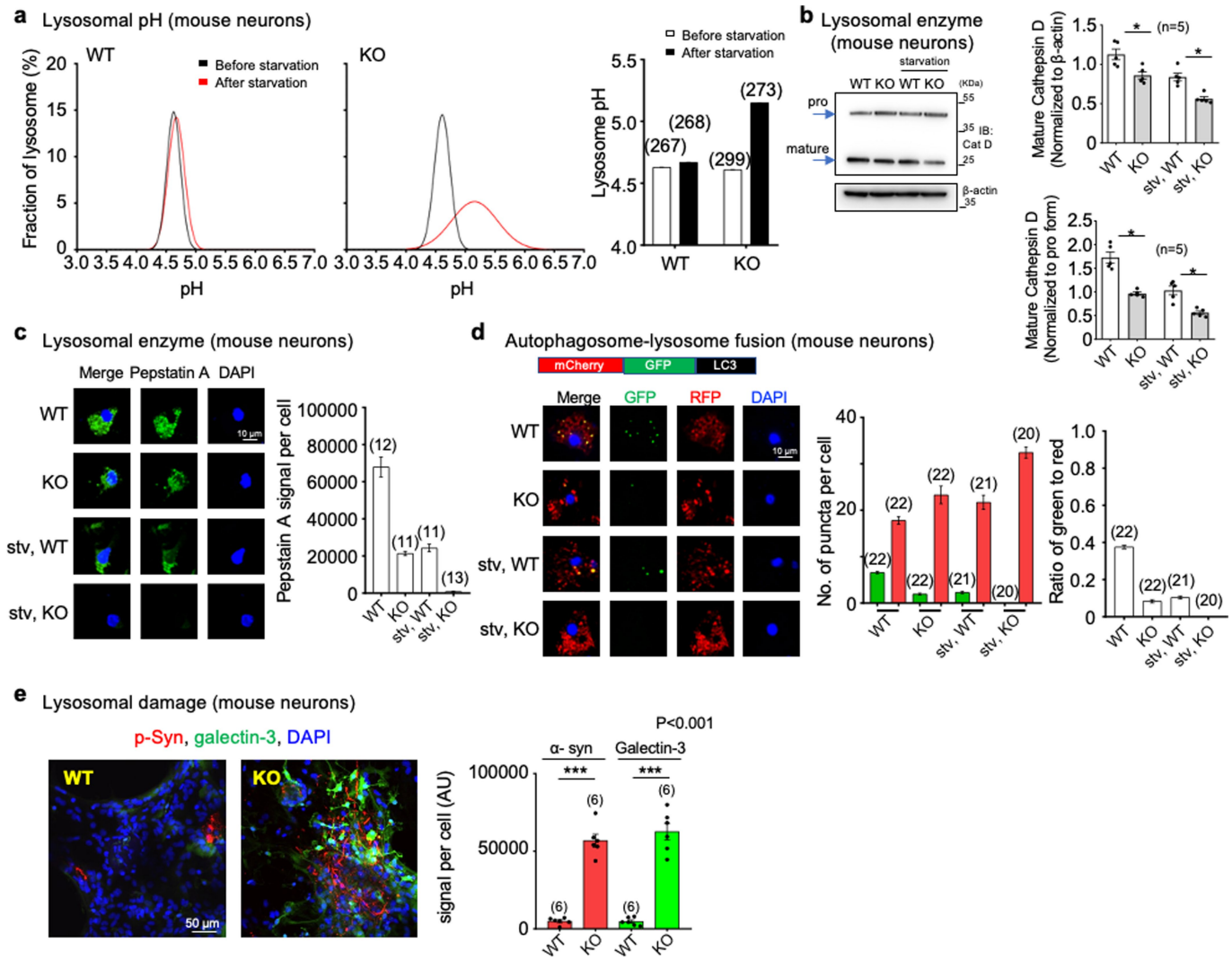

Extended Data Fig. 9 | TMEM175 contributes to lysosomal pH stability and membrane integrity, regulates lysosomal enzyme activity and controls organelle fusion during autophagy. a, Lysosomal pH from wild-type and TMEM175-knockout cultured mouse hippocampal neurons with or without starvation (overnight in DMEM). Distribution of pH values are in the first two subpanels. Average values are in the bar graph. Numbers of lysosomes analysed are in parentheses. **b**, Comparison of mature CatD levels using anti-CatD antibody. Lysate from cultured wild-type or TMEM175-knockout hippocampal neurons, with or without starvation, were probed with anti- CatD, or anti-β-actin for loading control. The mature form of CatD (bottom band) is cleaved from pro-CatD (top band) and the cleavage is pH-dependent. Left, representative blot. Right, signal density of mature CatD normalized to that of pro-CatD (bottom) or to that of β-actin (top). $n = 5$ repeats. $^*P \le 0.05$. P values (unpaired two-tailed t-test, wild type vs knockout) are as follows: normalized to β-actin, $P = 0.0119$ (without starvation), $P = 0.0011$ (with starvation); normalized to pro form, $P = 0.0002$ (without starvation), $P = 0.0015$ (with starvation). For gel source data, see Supplementary Fig. 1. **c**, Comparison of mature CatD levels using BODIPY FL pepstatin A (a fluorescent cathepsin indicator that binds to CatD in a pH-dependent manner). Cultured wild-type and TMEM175-knockout hippocampal neurons, with or without starvation, were treated with BODIPY FL pepstatin A (1 μM, 1 h) and imaged for pepstatin A and nuclei. Left, representative images of pepstain A (green), DAPI (blue) and merge between the two. Right, pepstain A signals normalized to numbers of cells (n, number of coverslips imaged). **d**, Autophagosome–lysosome fusion assay with an mCherry- and GFP-tagged LC3 (tandem tag, illustrated) transfected into wild-type and TMEM175-knockout hippocampus neurons with or without starvation. Left, representative images for GFP (indicative of autophagosome puncta before fusion with lysosome; GFP is invisible after fusion with lysosome because of its pH sensitivity), RFP (indicative of total number of autophagosome puncta before and after phagosome–lysosome fusion; RFP is visible under both neutral and acidic pH) and DAPI (nucleus), and merge among the three. Bar graph indicated averaged numbers of GFP and RFP puncta upon treatments as indicated (middle) and numbers of GFP-positive puncta normalized to those of RFP-positive ones (right). Number of cells analysed are in parentheses. **e**, Experiments demonstrating that deficiency in lysoK$_{GF}$ leads to accelerated spreading of pathogenic α-syn and lysosomal permeability in neurons. Cultured wild-type and TMEM175-knockout hippocampal neurons were seeded with mouse α-syn PFFs and costained with anti-pSer129 α-syn (pSyn, red) and anti-galectin 3 (green) two weeks later. DAPI (blue) nuclear staining was used to identify the number of cells. Representative images are in the left panels and averaged pSyn and galectin 3 signal density (normalized to number of cells) are in the right bar graph ($n = 6$ coverslips each). $^{***}P \le 0.001$.
P values (unpaired two-tailed t-tests; knock out versus wild type) are $P < 0.0001$ for α-syn and galectin 3. In the bar graphs, data are represented as mean ± s.e.m.

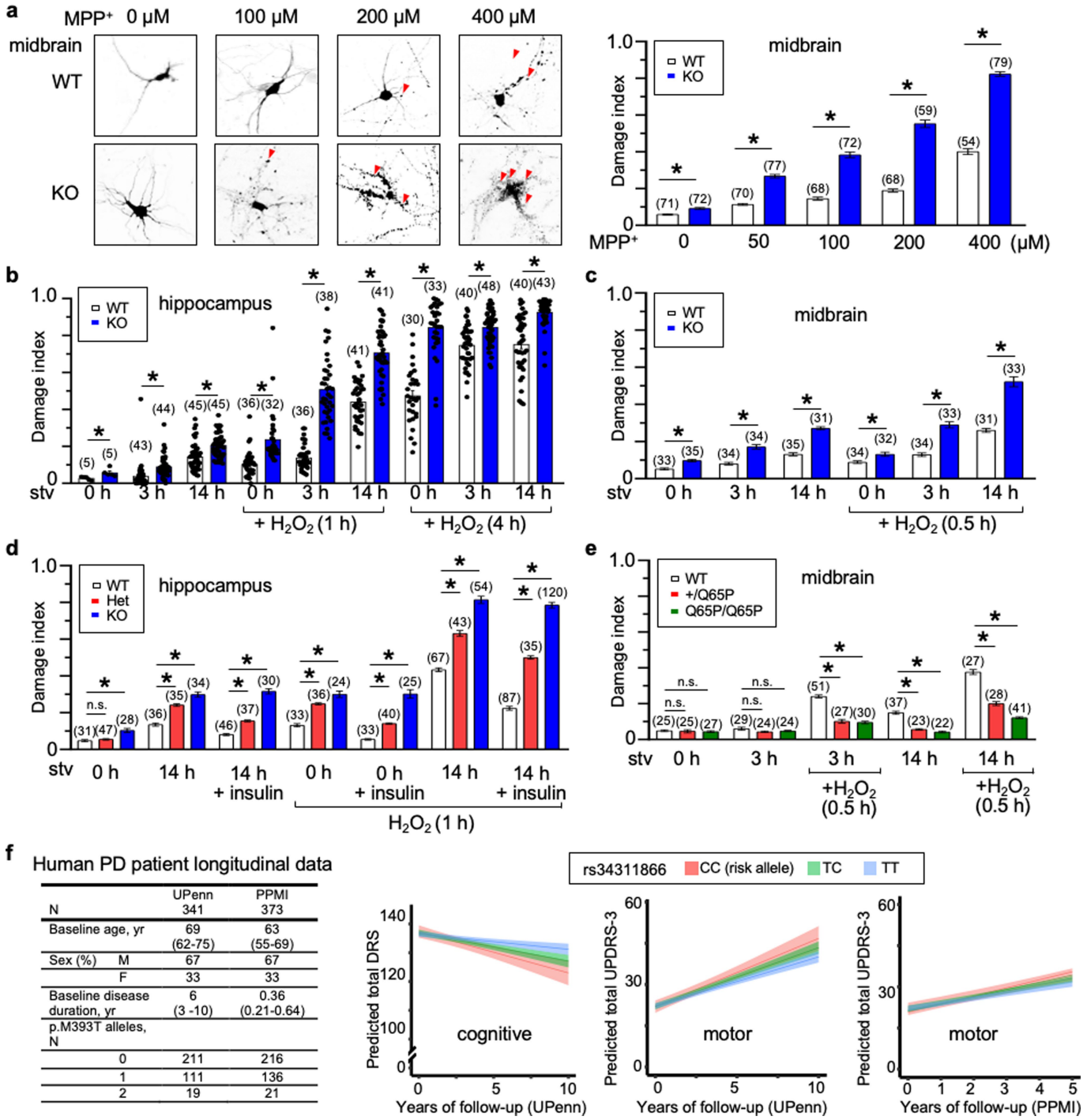

f

Human PD patient longitudinal data

		UPenn	PPMI
N		341	373
Baseline age, yr		69 (62-75)	63 (55-69)
Sex (%)	M	67	67
	F	33	33
Baseline disease duration, yr		6 (3 -10)	0.36 (0.21-0.64)
p.M393T alleles, N			
	0	211	216
	1	111	136
	2	19	21

Extended Data Fig. 10 | See next page for caption.

Extended Data Fig. 10 | LysoK$_{GF}$ protects mouse neurons from stress-induced damage in a gene-dosage-dependent manner, and a loss-of-function variant in the human *TMEM175* gene is nominally associated with increased rates of cognitive and motor function decline in patients with Parkinson's disease. a–**e**, Cultured mouse neurons were challenged with MPP$^+$ toxin, B27 deprivation (in DMEM) and/or H_2O_2 treatment. Images were taken for damage analysis. Blebs and fragmentation in neuronal processes were counted as damage, as indicated by arrows in representative pictures in **a**. The damage index was calculated as the ratio of damaged area to the total neuronal area. **a**, Treatment of wild-type and TMEM175-knockout midbrain neurons with MPP$^+$ added to culture medium for 12 h, with concentrations as indicated. Left, representative images of neurons with bleb damages indicated by arrows. Right, damage index. **b**, **c**, Hippocampal (**b**) or midbrain (**c**) neurons were starved in DMEM for duration as indicated. H_2O_2 (100 μM) treatment for the period indicated was carried out in DMEM after starvation. **d**, Effects of insulin. In the group of neurons treated with 14-h starvation and insulin, without H_2O_2, neurons were starved for 14 h in DMEM followed by incubation with insulin (100 nM in DMEM) for 3 h. In the groups treated with H_2O_2, neurons were starved in DMEM for 0 or 14 h, followed by a 3-h incubation with or without insulin (100 nM). During the last hour of incubation, H_2O_2 (100 μM) was added to the medium. **e**, Comparison between wild-type and TMEM175(Q65P)-carrying neurons with treatments similar to those in **c**. In the bar graphs, data are mean ± s.e.m.; numbers of neurons analysed are in parentheses. *$P \leq 0.05$. *P* values (unpaired two-tailed *t*-tests) are as follows. In **a**, wild type versus knockout: $P < 0.0001$ for all comparisons. In **b**, wild type versus knockout: $P = 0.0192$ (0 h, starved), $P = 0.0004$ (3 h, starved), $P < 0.0001$ for the other comparisons. In **c**, wild type versus knockout: $P = 0.0017$ (0 h + H_2O_2), $P < 0.0001$ for the other comparisons. In **d**, compared with wild type: $P = 0.264$ (HET, 0 h), $P < 0.0001$ for the other comparisons. In **e**, compared with wild type: $P = 0.8121$ (+/Q65P, 0 h), $P = 0.545$ (Q65P/Q65P, 0 h), $P = 0.0935$ (+/Q65P, 3 h), $P = 0.2012$ (Q65P/Q65P, 3 h), $P < 0.0001$ for the other comparisons. **f**, Clinical effect of the rs34311866 (p.M393T) variant in the human *TMEM175* on longitudinal course of Parkinson's disease. Longitudinal effects for carriers of no (blue), one (green), or two (red) p.M393T variants are shown for mixed-effects linear regression models without multiple testing correction; 95% confidence intervals are indicated by coloured bands. In the UPenn cohort, p.M393T carriers had faster cognitive decline (two-tailed $P = 0.005$, as captured by lower DRS-2 scores) and faster motor decline (two-tailed $P = 0.032$, higher UPDRS-3 scores). In the PPMI cohort, p.M393T carriers trended (two-tailed $P = 0.066$) towards faster motor decline, although no statistical significance was reached (presumably because of shorter observation period, of 5 years after diagnosis). As TMEM175 variants are associated with neurodegenerative diseases and AKT is known to protect neurons against stress-induced damage[25,35,36], we tested whether lysoK$_{GF}$ protects neurons. To do this, we used a neuronal culture model in which damage induced by insults such as the neurotoxin MPTP, H_2O_2 and nutrient removal can be quantified well[37–39]. MPTP interferes with mitochondrial metabolism, inducing parkinsonism in humans and in animal models[84]. Consistent with previous findings[85,86], incubating midbrain neurons with MPP$^+$ (the active form of the neurotoxin) led to perturbations and beading of neuronal processes in a dose-dependent manner. When the size of such damaged areas normalized to the total neuronal area (that is, damage index) was quantified, TMEM175-knockout neurons exhibited much more severe damage compared to wild type (**a**). Both nutrient removal and reactive oxygen species (such as H_2O_2) cause neuronal damage[39]. Under each combination of H_2O_2 treatment after B27 removal, TMEM175-knockout neurons exhibited more severe damage than wild type (**b**, **c**). Growth factors such as insulin are known to mitigate neuronal damage but the mechanisms are not well-understood[87]. In wild-type neurons, insulin reduced the damage induced by B27 removal and/or H_2O_2 treatment. Notably, this protection was nearly absent in TMEM175-knockout neurons (**d**), which suggests an essential role for TMEM175. In heterozygous neurons, the degree of damage was intermediate between that of wild-type and TMEM175-knockout neurons (**d**). Thus, *Tmem175* gene dosage has an incremental effect on neuronal protection. Decreasing $I_{TMEM175}$ by about 50% is sufficient to compromise the protection. In support of this finding, neurons from TMEM175(I390T) knock-in mice were also more prone to MPP$^+$-induced damage than were neurons from wild-type mice (Extended Data Fig. 8c). We also tested whether p.Q65P provides additional protection. When challenged with B27 deprivation and H_2O_2, neurons from both heterozygous (Q65P/+) and homozygous (Q65P/Q65P) mice had much less damage than those from wild type (**e**). The difference was even more notable between TMEM175(Q65P)-carrying neurons and TMEM175-knockout neurons. For example, after a 14-h starvation the TMEM175-knockout neurons had 27% damage and wild-type neurons had 15%—but those from *Tmem175*$^{Q65P/+}$ mice had only 6%. Similarly, H_2O_2-induced damages were mitigated in TMEM175(Q65P)-carrying neurons (**c**, **e**). These data suggest that p.Q65P is neuroprotective and constitutes a potential mechanism that underlies a reduced susceptibility to developing Parkinson's disease.

nature research

Corresponding author(s): Dejian Ren

Last updated by author(s): Nov 15, 2020

Reporting Summary

Nature Research wishes to improve the reproducibility of the work that we publish. This form provides structure for consistency and transparency in reporting. For further information on Nature Research policies, see Authors & Referees and the Editorial Policy Checklist.

Statistics

For all statistical analyses, confirm that the following items are present in the figure legend, table legend, main text, or Methods section.

n/a	Confirmed	
☐	☒	The exact sample size (*n*) for each experimental group/condition, given as a discrete number and unit of measurement
☐	☒	A statement on whether measurements were taken from distinct samples or whether the same sample was measured repeatedly
☐	☒	The statistical test(s) used AND whether they are one- or two-sided *Only common tests should be described solely by name; describe more complex techniques in the Methods section.*
☒	☐	A description of all covariates tested
☐	☒	A description of any assumptions or corrections, such as tests of normality and adjustment for multiple comparisons
☐	☒	A full description of the statistical parameters including central tendency (e.g. means) or other basic estimates (e.g. regression coefficient) AND variation (e.g. standard deviation) or associated estimates of uncertainty (e.g. confidence intervals)
☒	☐	For null hypothesis testing, the test statistic (e.g. *F*, *t*, *r*) with confidence intervals, effect sizes, degrees of freedom and *P* value noted *Give P values as exact values whenever suitable.*
☒	☐	For Bayesian analysis, information on the choice of priors and Markov chain Monte Carlo settings
☒	☐	For hierarchical and complex designs, identification of the appropriate level for tests and full reporting of outcomes
☒	☐	Estimates of effect sizes (e.g. Cohen's *d*, Pearson's *r*), indicating how they were calculated

Our web collection on statistics for biologists contains articles on many of the points above.

Software and code

Policy information about availability of computer code

Data collection	pClamp (version 10.4, Molecular Device), ImSpector Microscope Controller (Version 144, LaVision Biotec)
Data analysis	Clampfit (version 10.4, Molecular Device), Origin (version 8.0, Origin Lab), Imaris (version 8.0, Oxford Instruments), ImageJ (version 1.53a, US NIH), R (RStudio, Version 1.1.456)

For manuscripts utilizing custom algorithms or software that are central to the research but not yet described in published literature, software must be made available to editors/reviewers. We strongly encourage code deposition in a community repository (e.g. GitHub). See the Nature Research guidelines for submitting code & software for further information.

Data

Policy information about availability of data

All manuscripts must include a data availability statement. This statement should provide the following information, where applicable:

- Accession codes, unique identifiers, or web links for publicly available datasets
- A list of figures that have associated raw data
- A description of any restrictions on data availability

All relevant data and code are freely available from the authors. Figures 1-5 and Extended Data Figures 1-10 have raw data.
Parkinson's Progression Markers Initiative (PPMI) database: https://www.ppmi-info.org/access-data-specimens/, Genome Aggregation Database (gnomAD): https://gnomad.broadinstitute.org/, PD Gene database: http://www.pdgene.org/, PDB ID 6WCA: https://www.rcsb.org/structure/6WCA.

Field-specific reporting

Please select the one below that is the best fit for your research. If you are not sure, read the appropriate sections before making your selection.

☒ Life sciences ☐ Behavioural & social sciences ☐ Ecological, evolutionary & environmental sciences

For a reference copy of the document with all sections, see nature.com/documents/nr-reporting-summary-flat.pdf

Life sciences study design

All studies must disclose on these points even when the disclosure is negative.

Sample size	Sample sizes were not predetermined using statistical methods; they are chosen based on statistical analysis and standards in the field (e.g. Cang et. al. (2015) Cell 162:1101-12). See sections "Statistical analysis of clinical data" and "Other statistical information".
Data exclusions	No data were excluded from analyses.
Replication	All experiments were independently replicated at least in two indepependent preparations for electrophysiology and three times for protein chemistry experiments. See section "Other statistical information and reproducibility".
Randomization	Mice used in the behavioral studies were randomized. The electrophysiological and protein chemistry experiments were not as some of them are hard to be randomized.
Blinding	We did blind experiments for Fig. 1b, 1i (left panel), 2i(starvation experiment), 4d-f, 5a-d, Extended data Fig. 1a, Extended data Fig. 1d, Extended data Fig. 1e, Extended data Fig. 8b-d, Extended data Fig. 9a, Extended data Fig. 9c-e and Extended data Fig. 10a-e. The others were not blinded as blinding unlikely affects the results.

Reporting for specific materials, systems and methods

We require information from authors about some types of materials, experimental systems and methods used in many studies. Here, indicate whether each material, system or method listed is relevant to your study. If you are not sure if a list item applies to your research, read the appropriate section before selecting a response.

Materials & experimental systems

n/a	Involved in the study
☐	☒ Antibodies
☐	☒ Eukaryotic cell lines
☒	☐ Palaeontology
☐	☒ Animals and other organisms
☐	☒ Human research participants
☒	☐ Clinical data

Methods

n/a	Involved in the study
☒	☐ ChIP-seq
☒	☐ Flow cytometry
☒	☐ MRI-based neuroimaging

Antibodies

Antibodies used

β-actin (rabbit monoclonal, Cell Signaling Technology, #4970, 1:3000),
GFP (mouse monoclonal, Thermo Fisher Scientific, #A11120 1:1000; mouse monoclonal, Santa Cruz Biotechnology, #sc-9996, 1:2000),
TMEM175 (rabbit polyclonal, Proteintech, #19925-1-AP 1:1000; rabbit polyclonal, Origene, #TA335429, 2 μg/ml),
Akt (rabbit polyclonal, Cell Signaling Technology, #9272, 1:1000),
pan-Akt (mouse monoclonal, R&D Systems, #MAB2055, 0.2 ug/ml),
HA (mouse monoclonal, Santa Cruz Biotechnology, #sc-7392, 1:1000),
phospho-Akt (Ser473) (rabbit polyclonal, Cell Signaling Technology, #9271, 1:2000),
phospho-Akt (Thr308) (rabbit monoclonal, Cell Signaling Technology, #4056, 1:1000),
phospho-GSK3β (Ser9) (rabbit monoclonal, Cell Signaling Technology, #9323, 1:1000),
GSK3β (rabbit monoclonal, Cell Signaling Technology, #9315, 1:1000),
phospho-PRAS40(T246) (rabbit monoclonal, Cell Signaling Technology, #2691, 1:1000),
PRAS40 (rabbit monoclonal, Cell Signaling Technology, #2997, 1:1000,
cathepsin D (rabbit polyclonal, Cell Signaling Technology, #2284, 1:200).
rabbit IgG (Cell Signaling Technology, #7074, 1:4000),
mouse IgG (Abcam, #ab131368, 1:1000; Cell Signaling Technology, #7076, 1:4000),
VeritBlot for IP detection reagent (HRP) (Abcam, #ab131366, 1:4000),
pSer129 α-synuclein (mouse clone mAb 81A, 1:8000 {Waxman, 2008 #3214})
galectin-3 (rat monoclonal, 1:100, Santa Cruz Biotechnology, # sc-81728).
Alexa Fluor 594-conjugated goat anti-mouse secondary antibody (Thermo Fisher Scientific, #A-11032, 2 μg/ml)

Alexa Fluor 488-conjugated rabbit anti-α-tubulin antibody (Cell Signaling Technology, #5063S, 1:200),
Alexa Fluor 488 conjugated rabbit anti-rat secondary antibody (Thermo Fisher Scientific, #A-21210, 2 µg/ml).
DAT (rat monoclonal, Santa Cruz Biotechnology, #sc-32258, 1:500)
TH (rabbit polyclonal, Millipore Sigma, #AB-152, 1:500),
Alexa Fluor-conjugated secondary antibody (goat anti-rat IgG, Alexa 647, Thermo Fisher Scientific, #A21247, 1:500),
Alexa Fluor-conjugated secondary antibody (goat anti-rabbit IgG Alexa 647 (Thermo Fisher Scientific, #A21245, 1:500),
Tyrosine hydroxylase (Millipore Sigma, #TH-16; 1:5,000),
NeuN (Millipore Sigma, #A60; 1:1,000),
biotinylated anti-mouse IgG (1:1,000; Vector Laboratories, #BA2000),

Validation

β-actin (rabbit monoclonal, Cell Signaling Technology, #4970, 1:3000), https://www.cellsignal.com/products/primary-antibodies/b-actin-13e5-rabbit-mab/4970
GFP (mouse monoclonal, Thermo Fisher Scientific, #A11120 1:1000), https://www.thermofisher.com/antibody/product/GFP-Antibody-clone-3E6-Monoclonal/A-11120, validated against non-transfected cells.
GFP (mouse monoclonal, Santa Cruz Biotechnology, #sc-9996, 1:2000), https://www.scbt.com/p/gfp-antibody-b-2, validated against non-transfected cells.
TMEM175 (rabbit polyclonal, Proteintech, #19925-1-AP 1:1000), https://www.ptglab.com/products/TMEM175-Antibody-19925-1-AP.htm, validated against knockout.
TMEM175 (rabbit polyclonal, Origene, #TA335429, 2 µg/ml), https://www.origene.com/catalog/antibodies/primary-antibodies/ta335429/transmembrane-protein-175-tmem175-rabbit-polyclonal-antibody, validated against knockout.
Akt (rabbit polyclonal, Cell Signaling Technology, #9272, 1:1000), https://www.cellsignal.com/products/primary-antibodies/akt-antibody/9272
pan-Akt (mouse monoclonal, R&D Systems, #MAB2055, 0.2 ug/ml), https://www.rndsystems.com/products/human-mouse-rat-akt-pan-specific-antibody-281046_mab2055
HA (mouse monoclonal, Santa Cruz Biotechnology, #sc-7392, 1:1000), https://www.scbt.com/p/ha-probe-antibody-f-7, validated against non-transfected cells.
phospho-Akt (Ser473) (rabbit polyclonal, Cell Signaling Technology, #9271, 1:2000), https://www.cellsignal.com/products/primary-antibodies/phospho-akt-ser473-antibody/9271, validated against starved cells.
phospho-Akt (Thr308) (rabbit monoclonal, Cell Signaling Technology, #4056, 1:1000), https://www.cellsignal.com/products/primary-antibodies/phospho-akt-thr308-244f9-rabbit-mab/4056, validated against starved cells.
phospho-GSK3β (Ser9) (rabbit monoclonal, Cell Signaling Technology, #9323, 1:1000), https://www.cellsignal.com/products/primary-antibodies/phospho-gsk-3b-ser9-5b3-rabbit-mab/9323, validated against starved cells.
GSK3β (rabbit monoclonal, Cell Signaling Technology, #9315, 1:1000), https://www.cellsignal.com/products/primary-antibodies/gsk-3b-27c10-rabbit-mab/9315
phospho-PRAS40(T246) (rabbit monoclonal, Cell Signaling Technology, #2691, 1:1000), https://www.cellsignal.com/products/primary-antibodies/pras40-d23c7-xp-rabbit-mab/2691, validated against starved cells.
PRAS40 (rabbit monoclonal, Cell Signaling Technology, #2997, 1:1000, https://www.cellsignal.com/products/primary-antibodies/phospho-pras40-thr246-c77d7-rabbit-mab/2997
cathepsin D (rabbit polyclonal, Cell Signaling Technology, #2284, 1:200), https://www.cellsignal.com/products/primary-antibodies/cathepsin-d-antibody/2284
HRP conjugated rabbit IgG (Cell Signaling Technology, #7074, 1:4000), https://www.cellsignal.com/products/secondary-antibodies/anti-rabbit-igg-hrp-linked-antibody/7074
mouse IgG (Abcam, #ab131368, 1:1000; Cell Signaling Technology, #7076, 1:4000), https://www.cellsignal.com/products/secondary-antibodies/anti-mouse-igg-hrp-linked-antibody/7076
VeritBlot for IP detection reagent (HRP) (Abcam, #ab131366, 1:4000), https://www.abcam.com/veriblot-for-ip-detection-reagent-hrp-ab131366.html
pSer129 α-synuclein (mouse clone mAb 81A, 1:8000 (Waxman et al. Specificity and regulation of casein kinase-mediated phosphorylation of alpha-synuclein, J Neuropathol Exp Neurol. 2008 May;67(5):402-16. doi: 10.1097/NEN.0b013e31816fc995)
galectin-3 (rat monoclonal, 1:100, Santa Cruz Biotechnology, #sc-81728), https://www.scbt.com/p/galectin-3-antibody-m3-38-1-2-8-hl-2
Alexa Fluor 594-conjugated goat anti-mouse secondary antibody (Thermo Fisher Scientific, #A-11032, 2 µg/ml), https://www.thermofisher.com/antibody/product/Goat-anti-Mouse-IgG-H-L-Highly-Cross-Adsorbed-Secondary-Antibody-Polyclonal/A-11032
Alexa Fluor 488-conjugated rabbit anti-α-tubulin antibody (Cell Signaling Technology, #5063S, 1:200), https://www.cellsignal.com/products/antibody-conjugates/a-tubulin-11h10-rabbit-mab-alexa-fluor-488-conjugate/5063?Ntk=Products&Ntt=5063
Alexa Fluor 488 conjugated rabbit anti-rat secondary antibody (Thermo Fisher Scientific, #A-21210, 2 µg/ml), https://www.thermofisher.com/antibody/product/Rabbit-anti-Rat-IgG-H-L-Cross-Adsorbed-Secondary-Antibody-Polyclonal/A-21210
DAT (rat monoclonal, Santa Cruz Biotechnology, #sc-32258, 1:500), https://www.scbt.com/p/dat-antibody-6-5g10
TH (rabbit polyclonal, Millipore Sigma, #AB-152, 1:500), https://www.sigmaaldrich.com/catalog/product/mm/ab152?lang=en&region=US&gclid=Cj0KCQiA-rj9BRCAARIsANB_4ADs7HEZA0dDtXIvjHo9R01UpsGTb3p-JbYAvodrrN-7bQnPVPE87BoaAjrZEALw_wcB
Alexa Fluor-conjugated secondary antibody (goat anti-rat IgG, Alexa 647, Thermo Fisher Scientific, #A21247, 1:500), https://www.thermofisher.com/antibody/product/Goat-anti-Rat-IgG-H-L-Cross-Adsorbed-Secondary-Antibody-Polyclonal/A-21247
Alexa Fluor-conjugated secondary antibody (goat anti-rabbit IgG Alexa 647 (Thermo Fisher Scientific, #A21245, 1:500), https://www.thermofisher.com/antibody/product/Goat-anti-Rabbit-IgG-H-L-Highly-Cross-Adsorbed-Secondary-Antibody-Polyclonal/A-21245
Tyrosine hydroxylase (Millipore Sigma, #TH-16; 1:5,000), https://www.bosterbio.com/anti-tyrosine-hydroxylase-antibody-monoclonal-ma1100-boster.html
NeuN (Millipore Sigma, #A60; 1:1,000), https://www.emdmillipore.com/US/en/product/Anti-NeuN-Antibody-clone-A60,MM_NF-MAB377
biotinylated anti-mouse IgG (1:1,000; Vector Laboratories, #BA2000), https://vectorlabs.com/biotinylated-horse-anti-mouse-igg-antibody.html

Eukaryotic cell lines

Policy information about cell lines

Cell line source(s)	HEK293T and SH-SY5Y from ATCC and S2 cell from Gibco, described in section "Cell Culture".
Authentication	The cell lines were purchased and authenticated by the providers (ATCC and Gibco); we did not carry out additional authentificaiton.
Mycoplasma contamination	HEK293T and SH-SY5Y from ATCC, and S2 cell from Gibco were tested by the providers.
Commonly misidentified lines (See ICLAC register)	No commonly misidentified cell line was used in this study.

Animals and other organisms

Policy information about studies involving animals; ARRIVE guidelines recommended for reporting animal research

Laboratory animals	Wild-type and mutant mice (BL6 background) were used, as described in the section "Animals". Description of research mice used for each experiments can be found in the relevant figure legends. Neuronal cultures were made from P0 pups with genders undetermined. Brain proteins used work for immunoprecipitation and Western blot were collected from 3-5 month old mice (mixture of male and females) Behavior and Immunostaining comparing WT and heterozygous littermates used mice of ~12 months old (both males and females). Immunostaining comparing WT and homozygous KO littermates used mice of 18-22 months old (both males and females). Average temperature in the housing rooms was 72 degree F; humidity was approximately 40%. Light cycle was 12 hours light/12 hours dark.
Wild animals	No wild animal was used.
Field-collected samples	No field-collected sample was used.
Ethics oversight	Animal use was approved by the The University of Pennsylvania's IACUC, The Animal Care and Use Committee of the School of Medicine at Fudan University, The clinical studies were approved by The University of Pennsylvania (UPenn) Institutional Review Board

Note that full information on the approval of the study protocol must also be provided in the manuscript.

Human research participants

Policy information about studies involving human research participants

Population characteristics	UPenn: Participants included male and female patients (defined as biological sex assigned at birth), 50 years of age and older, diagnosed with Parkinson's disease based on UK Brain Bank Criteria by a movement disorders neurologist, prospectively enrolled at the University of Pennsylvania Parkinson's Disease and Movement Disorders Center (Philadelphia, PA). See section "Human clinical studies". PPMI: Participants included people with a diagnosis of PD for two years or less who are not taking PD medications. Please see https://www.ppmi-info.org/study-design/study-cohorts/ for more information.
Recruitment	UPenn: Participants were recruited by a movement disorders neurologist during a regularly schedule clinical office visit at the University of Pennsylvania Parkinson's Disease and Movement Disorders Center (Philadelphia, PA). All patients seen at the Parkinson's Disease and Movement Disorders Center with a diagnosis of Parkinson's disease were eligible to participate. Self-selection bias may be present in this cohort, although it is unlikely to have a significant impact on longitudinal cognitive or motor progression; Participants in this study were prospectively enrolled. See section "Human clinical studies". PPMI: Please see https://www.ppmi-info.org/study-design/study-cohorts/ for more information.
Ethics oversight	University of Pennsylvania (UPenn) Institutional Review Board

Note that full information on the approval of the study protocol must also be provided in the manuscript.